Doctoral Dissertation

In Pursuit of Depression Biomarkers: Exploring the Neural Energy Landscapes of Melancholic Depression

Paul Rossener R. Regonia
Program of Data Science
Graduate School of Science and Technology
Nara Institute of Science and Technology

Supervisor: Prof. Kazushi Ikeda
Mathematical Informatics Lab (Division of Information Science)

16 March 2022

A Doctoral Dissertation
submitted to Graduate School of Science and Technology,
Nara Institute of Science and Technology
in partial fulfillment of the requirements for the degree of
Doctor of Science

Paul Rossener R. Regonia

Thesis Committee:

Supervisor Kazushi Ikeda
(Professor, Division of Information Science)

Shigehiko Kanaya
(Professor, Division of Information Science)

Hisao Yanagi
(Professor, Division of Materials Science)

Junichiro Yoshimoto
(Associate Professor, Division of Information Science)

Makoto Fukushima
(Assistant Professor, Division of Information Science)

Jaymar B. Soriano
(Assistant Professor, University of the Philippines Diliman)

Greg J. Siegle
(Professor, University of Pittsburgh School of Medicine)

Tetsuya Yamamoto
(Associate Professor, Tokushima University)

In Pursuit of Depression Biomarkers: Exploring the Neural Energy Landscapes of Melancholic Depression*

Paul Rossener R. Regonia

Abstract

Neurodynamic biomarkers are crucial for accurate diagnosis and effective treatment of mental illnesses. Depression biomarker research has been active now, more than ever before. However, current neurodynamic biomarkers for MDD are based on functional connectivity (FC), which cannot capture higher-order interactions between multiple brain regions. Our goal is to find potential biomarkers for major depressive disorder (MDD), a debilitating disorder that has a worldwide impact.

This thesis introduces energy landscape analysis (ELA), a data-driven framework for modeling multilevel brain network dynamics of resting-state fMRI depression data using Pairwise Maximum Entropy Model (P-MEM). We explore different frameworks for characterizing depression. One is a singular model framework focused on building an unbiased baseline for classifying depressed individuals. Another is a separate model for melancholic depression, a subtype of depression known for greater severity. In our pursuit of MDD biomarkers, we find distinctive neurodynamics of melancholic depression, enriching our understanding of depression heterogeneity and ways to confront it.

Keywords:

depression, melancholia, energy landscape analysis, resting state fMRI, functional brain network, neurodynamics

*Doctoral Dissertation, Graduate School of Science and Technology, Nara Institute of Science and Technology, 16 March 2022.

Contents

List of Figures

List of Tables

1 Introduction

Depression is a universal human experience that has changed its meaning throughout history [1–4]. The earliest reference to depression roots back to the fourth century BC, when it was regarded by Hippocrates as *melancholia* — a mental disorder caused by an excess of black (*melan*) bile (*cholē*) that disrupts the humoral balance needed to maintain good health [1–5]. This humor-based concept of melancholia was adapted in the first century AD by physician Galen of Pergamum, who explained how the black bile might affect different parts of the body (such as the hypochondrium and the brain) and how this would lead to different subtypes of melancholia [4, 6].

By the onset of the 20th century, the term melancholia has evolved to denote a depressive state occurring in manic depression [1–4, 7]. Kraepelin, who has classified psychosis into either manic depression (bipolar disorder) or dementia praecox (schizophrenia), pioneered the systematic classification of mental disorders. At the same time, Freud has taken a psychological approach to analyze depression [1–4]. In *Mourning and Melancholia*, Freud compared depression and grief as a response to loss. Grief was a natural reaction to losing a loved one. In contrast, depression involved an idealized form of loss unknown to the person [8].

The myriads of theories on melancholia and depression called for standardization and uniformity. Meyer proposed *depression* as the official term to be used in the medical vocabulary, shunning the term *melancholia* as it has been afflicted with different meanings [9]. This proposal influenced the creation of the Diagnostic and Statistical Manual of Mental Disorders (DSM), which thoroughly details our modern concept of depression as a mental disorder [3, 4].

DSM has set the standard for the clinical diagnosis of psychiatric disorders. Its latest edition, DSM-V, lists at least six different types of depressive disorder, the most common of which is major depressive disorder (MDD) [10]. Currently,

Table 1.1: Major depressive disorder symptoms, DSM-V

(1)	Depressed mood most of the day (e.g., feels sad, empty, hopeless)*
(2)	Markedly diminished interest or pleasure in activities most of the day*
(3)	Significant weight loss when not dieting, or weight gain, or decrease or increase in appetite
(4)	Insomnia or hypersomnia
(5)	Psychomotor agitation or retardation
(6)	Fatigue or loss of energy
(7)	Feelings of worthlessness or excessive or inappropriate guilt
(8)	Diminished ability to think or concentrate, or indecisiveness
(9)	Recurrent thoughts of death (not just fear of dying), suicidal ideation without a specific plan, a suicide attempt or a specific plan for committing suicide

** must have either of these*

a person is diagnosed with MDD if they experience at least five out of nine symptoms determined by DSM-V within two weeks (Table 1.1). Diagnosis is typically made by interviewing the patient, in which the patient answers an itemized questionnaire, with each item corresponding to specific symptoms. Questionnaires vary from assessing depression severity (Beck Depression Inventory, or BDI-II [11]), to evaluating comorbidity of psychiatric disorders (Mini-International Neuropsychiatric Interview, or MINI [12]).

1.1 Finding biomarkers for depression

The primary purpose of diagnosis is to provide proper treatment. Thus, it is equally important to correctly detect the presence of depression and predict the degree of severity to administer the right amount of treatment. In this regard, symptoms-based diagnostic tools such as DSM-V may tend to overgeneralize depression [13, 14]. DSM-V classifies disorders in symptoms expression, comorbidity, and familial patterns [15]. When assessing depression severity, the patient's interview scores for each symptom are summed and evaluated using a severity

Table 1.2: Depression severity scale, BDI-II

0-13	Healthy / minimal depression
14-19	Mild depression
20-28	Moderate depression
29-63	Severe depression

scale such as BDI-II depression rating (Table 1.2) [11]. However, this approach only works if the symptoms are equally good indicators of severity, which is not the case for depression due to its heterogeneous nature [13, 14].

Depression heterogeneity is a major stumbling block to progress in depression research [14, 16–21]. This problem is partly due to the symptoms-based approach to classifying depression, which evaluates patients having contrasting symptoms with the same diagnosis. For example, DSM-V criteria for depression unequivocally classify a person with insomnia and losing weight and a person with hypersomnia but gaining weight as both having MDD. This scenario is a problem since the treatment for each should differ, yet DSM-V may fail to capture such information [18].

Depression biomarkers can help solve this heterogeneity problem by revealing the underlying mechanisms that give rise to the heterogeneous aspects of depression [16, 21]. These biomarkers can clarify the neurobiological substrates for depression [16], which can be used to define MDD subtypes [16, 19], and to predict clinical outcomes of various treatments [17, 20].

The importance of depression biomarkers clearly cannot be overstated. However, the complete characterization of biomarkers for clinical application is a conscientious process that requires rigorous cross-testing for preclinical sensitivity, specificity, reproducibility [22]. Thus, the scope of this study is limited to qualifying exploration biomarkers for MDD, where we perform our analyses without necessarily seeking pieces of evidence for clinical outcomes (Figure 1.1).

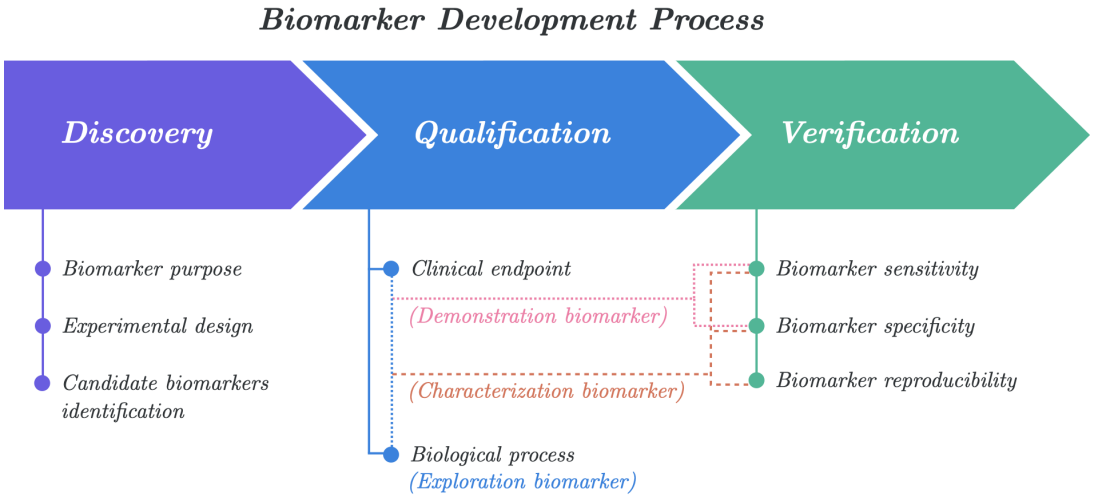

Figure 1.1: Stages of the biomarker development process [22]

The following section will discuss the existing analysis tools for depression biomarker discovery. Afterward, we will identify the gaps in this research field and propose our solution to bridging these gaps.

1.2 Existing approaches

Recent progress on depression biomarker research has shown promising results [20]. These biomarkers were derived from various sources such as inflammatory proteins [23], growth factors [24], metabolic factors [25], neurotransmitters [26], and neuroimaging data [16, 17, 19]. The challenge is consistency in findings since each source focuses on a unique facet of information when inspected.

Neuroimaging studies have provided shreds of evidence, both in structural and functional capacity, for the biological bases of MDD [19, 21]. Several meta-analyses have demonstrated consistent results across multiple independent neuroimaging studies [21], suggesting that data-driven neuroimaging models can be developed robustly against heterogeneous depression data [19].

Most neuroimaging studies utilize electroencephalography (EEG) or functional magnetic resonance imaging (fMRI) devices. EEG has the benefit of high temporal resolution that is useful for studying dynamic brain processes but has limited spatial resolution required for understanding the neural sources of these processes [27]. On the other hand, fMRI takes significantly longer time windows than EEG, which might miss the rapid neural activities involved in cognitive and perceptual processes. However, its highly localized spatial resolution can detect activations of specific brain regions in orders of magnitude higher than EEG [27]. Nevertheless, neuronal activations caused by cognitive tasks or stimuli are reflected as changes in blood oxygen level-dependent (BOLD) signals, which can then be detected by fMRI [28].

Much research towards analyzing neuroimaging biomarkers for MDD focused on building functional connectivity (FC) models of brain regions [29–35]. Seed-based functional connectivity analysis (which we will refer to as FCA) seeks temporal correlations between pairs of simultaneously activated brain regions, one of which is the seed [30, 32, 33]. Contrary to structural connectivity analysis (SCA), which reports actual anatomical connectivity of brain networks, FCA finds interactions between regions that may not be directly connected [30, 32, 33]. Despite their technical differences, several studies have demonstrated a connection between functional and structural alterations in MDD [30].

With the growing body of knowledge derived from FCA studies, we obtained a broader albeit muddled picture of MDD. First, these studies informed us about relevant brain regions associated with depression. Alterations in FC of brain regions such as default mode network (DMN) [30, 31, 34, 35], salience network (SN) [30, 31, 34, 36], and executive control network (ECN) [29–31, 34] were consistently reported.

Second, we also learned about MDD-related dynamic changes in the brain during task trials or at rest. The results varied depending on the task (e.g., cognitive, emotional, perceptive) and the regions of interest (ROIs) being analyzed [30, 32]. However, these studies have consistently shown decreased brain activity of MDD patients during task-based experiments compared to resting-state

scenarios [30], supporting the claim that MDD is a product of cognitive and emotional dysfunctionality [30, 34]Therefore, analyzing resting-state FC—commonly via resting-state fMRI (rsFMRI)—would eliminate the external stimuli factors that may otherwise be of little consequence to depressive processes such as introspection, rumination, and negative thinking.

Although there has been considerable development on FCA for discovering depression biomarkers, still, there are spaces for us to fill. The ability of FCA to reveal functional connections involved in specific cognitive processes is grounded on the assumption that pairwise interactions between the brain regions are independent [37, 38]. This assumption limits the capacity of FC-based models to capture global activity patterns involving multiple regions that are activated simultaneously [37, 38]. An alternative to seed-based FCA is independent component analysis (ICA) which captures large-scale network patterns but does not reveal connectivity patterns between networks [38]. For this reason, we developed a Pairwise Maximum Entropy Model (P-MEM) for MDD.

1.3 Our approach

P-MEM has been shown to accurately detect large-scale brain activities that are often overlooked by FCA [37]. At the same time, P-MEM estimates both individual activities and pairwise interactions of the ROIs being analyzed, allowing a closer inspection of the local, regional interactions that may otherwise be hidden from a global perspective [37, 39, 40]. Another advantage of P-MEM over FCA is the avoidance of seed selection. FCA is highly dependent on the seed ROI determined a priori, so changing the seed ROI would affect the results, which makes the analysis prone to bias [33]. P-MEM evades this problem by using a data-driven approach, something similar to ICA, where every possible pair of ROI are analyzed without a priori assumptions [33]. We use P-MEM as the primary model framework in this study for such reasons.

The second aspect of our modeling framework involves resting-state neu-

roimaging data. There are several benefits of using resting-state instead of task-induced data for modeling MDD. First, resting-state networks may be linked to non-stimulus-driven brain activities such as introspection and self-referential processing [30]. Second, although it may be counter-intuitive as the *resting* term implies, resting-state networks have been able to represent MDD-related dynamic brain patterns such as rumination [31], emotion dysregulation [32], and decreased reward anticipation [36] in cortical and subcortical regions. This representation power of resting-state networks is practically essential since the collection of resting-state data (such as rs-fMRI) is relatively easier to implement than task-based experiments and is more applicable across different age, gender, and culture groups. Moreover, P-MEM can approximate resting-state brain networks with high accuracy [37].

For the third and core aspect of our approach towards depression biomarker discovery, we introduce energy landscape analysis (ELA) — a computational model that borrows concepts from statistical physics, thermodynamics, and information theory [41–45]. In ELA, the brain is characterized as a dynamic system that switches between multiple stable states [46]. Each state is defined with energy; the higher the probability of a state to occur, the lower its energy will be. Due to the principle of minimal energy, the brain will tend to visit states with the lowest energy. Thus, these states are defined as stable states since they serve as equilibrium goalposts for the brain to achieve. They are also called *basins* on a similar tone, portraying the lowest points to which any object would reach in a landscape.

To date, ELA has not yet been used to model MDD, nor any of its subtypes, which is quite surprising since the visual connotation of energy landscape fits well with specific illustrations of depressive states such as being stuck in a state of negativity [2, 47, 48] or tottering on the edge of instability [2, 47, 49]. Our priority in this study is to find neurodynamic features that would serve as accurate biomarkers and explain the brain processes involved in depression. Thus, ELA is an appropriate approach to building an interpretable model for MDD.

We discuss the topics of energy landscapes, resting-state networks, and the

pairwise interaction model in *Chapter 2 - Materials and Methods*. Then, we report our initial findings in *Chapter 3 - Singular Model for Depression Biomarker*. Here, we also discuss the challenges with our initial model and our decision to explore a different but related problem. *Chapter 4 - Separate Model for Major Depression* and *Chapter 5 - Segregated Model for Melancholic Depression* examine these new frameworks and highlight the novel results. In *Chapter 6 - Discussions and Limitations* we follow through with a discussion of the results, the connections with depressive symptoms, and the limitations of our current model. Finally, in *Chapter 7 - Conclusion*, we trace our steps to our original goal of finding depression biomarkers and share our plans to achieve this further.

2 Materials and Methods

The human brain is a multistable system where, even at rest, it transitions between multiple stable states [46]. Our goal then is to unravel the transitional dynamics of the depressed brain—how it moves along these stable stables—to develop biomarkers for MDD. This section lays out the materials and methods we used to obtain this goal.

2.1 Study participants

Neuroimaging data were collected from healthy and depressed volunteers recruited since 2012 in four medical institutions in Hiroshima, Japan [50]. Before administering any experimental procedure, written informed consent was obtained from all participants. The experiments were carried out under relevant guidelines and regulations, and all experimental protocols were approved by the Ethics Committee of Hiroshima University. The mental condition of the volunteers was evaluated using Mini International Neuropsychiatric Interview (MINI) according to the Diagnostic and Statistical Manual of Mental Disorders, 4th ed. (DSM-IV) criteria [51]. InitialInitial screening resulted in 281 healthy participants with no history of mental or neurological disorder and 281 diagnosed with major depressive disorder (MDD). Among the healthy participants, some were reported as having potential mental disorder symptoms during the MINI interview (see Table A.1). However, we confirmed that they did not have psychiatric problems when further examined by psychiatrists.

Additional screening of participants was performed to emphasize the boundary between groups in the data set. First, the participants were screened based on their Beck Depression Inventory-II scores (BDI-II; healthy ≤ 13; depressed ≥ 20,

Table 2.1: Demographic data of healthy and depressed participants

	Healthy	Depressed	P-value
No. of participants	142	120	
Sex (female / male)[1]	71 / 71	60 / 60	
Age (years)[2]	42.62 ± 14.33	42.88 ± 11.12	
BDI-II[2]	5.34 ± 3.76	31.58 ± 7.57	(∗∗∗)
Anhedonia (SHAPS)[2]	23.27 ± 6.20	36.85 ± 6.17	(∗∗∗)
IQ (JART)[2]	110.92 ± 8.81	112.25 ± 9.39	
Site participants (HUH/HRC/HKH/COI)[1]	44 / 32 / 20 / 46	58 / 13 / 20 / 29	(∗∗)
Time samples per participant	161.90 ± 45.51	155.73 ± 43.31	

BDI-II, Beck Depression Inventory-II; SHAPS, Snaith-Hamilton Pleasure Scale; JART, Japanese Adult Reading Test

Recruitment sites: Hiroshima University Hospital (HUH), Hiroshima Rehabilitation Center (HRC), Hiroshima Kajikawa Hospital (HKH), Center of Innovation in Hiroshima University (COI)

[1] Pairwise Chi-squared test; [2] Wilcoxon-Mann-Whitney test; (∗∗) $p < 0.01$; (∗∗∗) $p < 0.005$

see Table 1.2) [11]. Second, participants were removed if they had incomplete data during the interview or excessive head movements during fMRI recording. Third, healthy female participants were randomly sampled to match the number of healthy males. The number of depressed male and female participants was already equal and need not be sampled randomly.

In the end, a total of 142 healthy (71 F / 71 M) and 120 depressed (60 F / 60 M) participants were screened and selected for analysis. After testing for statistical differences in age, sex, and other factors, significant differences were found in depression severity (BDI-II) and anhedonia (SHAPS) scores between the two groups. The distribution of participants across the four fMRI recording sites was significantly different as well. Details on the demographic data of participants are summarized in Table 2.1.

2.2 Resting-state fMRI data

The activation of neurons is driven by a process called the hemodynamic response, which supplies oxygen and increases the blood flow in the neuronal re-

gion. This process results in a difference in oxyhemoglobin and deoxyhemoglobin levels, which MRI can detect based on their magnetic susceptibilities. Thus, MRI is also called blood-oxygen-level-dependent (BOLD) contrast imaging [33]. Functional MRI utilizes the fluctuations in BOLD signals by mapping different—and not necessarily adjacent—brain regions based on their activation during specific tasks or reactions to particular stimuli. These fluctuations usually have a low frequency (0.01–0.1Hz) and are different from neural firings with higher frequency [33]. Nevertheless, fMRI has been widely used in neuropsychiatric studies due to its ability to detect synchronous activities of multiple brain regions [33, 52].

Despite initially being associated with a task- or stimulus-based paradigm, fMRI data can also be acquired without a task or stimulus. Known as resting-state fMRI (rs-fMRI), this type of fMRI data has been shown to have a good signal-to-noise ratio, can be administered to patients with physical disabilities, and translates well to clinical applications [33, 53, 54]. In this study, the rs-fMRI data of the participants were recorded using gradient echo-planar imaging (EPI) sequences. The imaging device and parameters differ depending on the recording site [50]. During recording, participants were instructed to focus on a cross mark displayed on a monitor and avoid thinking of anything or falling asleep. The fMRI recording lasted 5 to 10 minutes, depending on the recording site (Table 2.2).

Data preprocessing for the rs-fMRI data was performed using SPM8 (Wellcome Trust Centre for Neuroimaging, University College London, UK) on Matlab (Mathworks inc., USA). The preprocessing procedure included band-pass filtering (0.008–0.1 Hz), slice-timing correction, mean image realignment, normalization and resampling through segmentation of structural image aligned with the mean functional image, and smoothing with an isotropic 6mm full-width half-maximum Gaussian kernel [50, 55]. The potential confounding effects such as temporal fluctuations of white matter and cerebrospinal fluid, global signal, and six head motion parameters were linearly regressed out from the fMRI time series to remove the physiological noise and motion artifacts [56, 57]. These components were determined by the T1 images, which were simultaneously recorded with the rs-fMRI data. Finally, head motion artifacts were scrubbed from the functional mages based on the relative changes (i.e., translational displacements along X,

Table 2.2: Imaging protocols for different fMRI recording sites in Hiroshima

	HUH	HRC	HKH	COI
MRI scanner	GE Signa HDxt	GE Signa HDxt	Siemens Spectra	Siemens Verio
Magnetic field strength (T)	3.0	3.0	3.0	3.0
Channels per coil	8	8	12	12
Field of view (mm)	256 x 256	256 x 256	192 x 192	212 x 212
Matrix	64 x 64	64 x 64	64 x 64	64 x 64
Number of slices	32	32	38	40
Number of volumes	143	143	107	240
In-plane resolution (mm)	4.0 x 4.0	4.0 x 4.0	3.0 x 3.0	3.3125 x 3.3125
Slice thickness (mm)	4.0	4.0	3.0	3.2
Slice gap (mm)	0.0	0.0	0.0	0.8
TR (ms)	2.0	2.0	2.7	2.5
TE (ms)	27.0	27.0	31.0	30.0
Total scan time (min)	5	5	5	10
Flip angle (deg)	90	90	90	80
Slice acquisition order	Ascending (interleaved)	Ascending (interleaved)	Ascending (interleaved)	Ascending

Recruitment sites: Hiroshima University Hospital (HUH), Hiroshima Rehabilitation Center (HRC), Hiroshima Kajikawa Hospital (HKH), Center of Innovation in Hiroshima University (COI).

Y, and Z axes, and rotational displacements of pitch, yaw, and roll) between the image frames through time, with a frame-wise displacement (FD) threshold $= 0.5mm$ [58].

2.3 Functional brain networks

When selecting the ROIs for analysis, we considered functional brain networks associated with depression. Time-series data were extracted from 74 ROIs according to the 90-ROI Shirer Brain Atlas (Figure 2.1) [59], which includes brain networks such as default mode, executive control, and salience networks that have been linked to functional brain network analyses on depressive symptoms [29–32, 34–36]. Sixteen (16) ROIs were excluded due to either unreliable images during recording (e.g., in cerebellum area) [60], or an insufficient number of ROIs of corresponding functional networks (e.g., primary and higher visual networks). When extracting the time series data, the global mean and confounding effects of both cerebrospinal fluid (CSF) and white matter were linearly regressed out

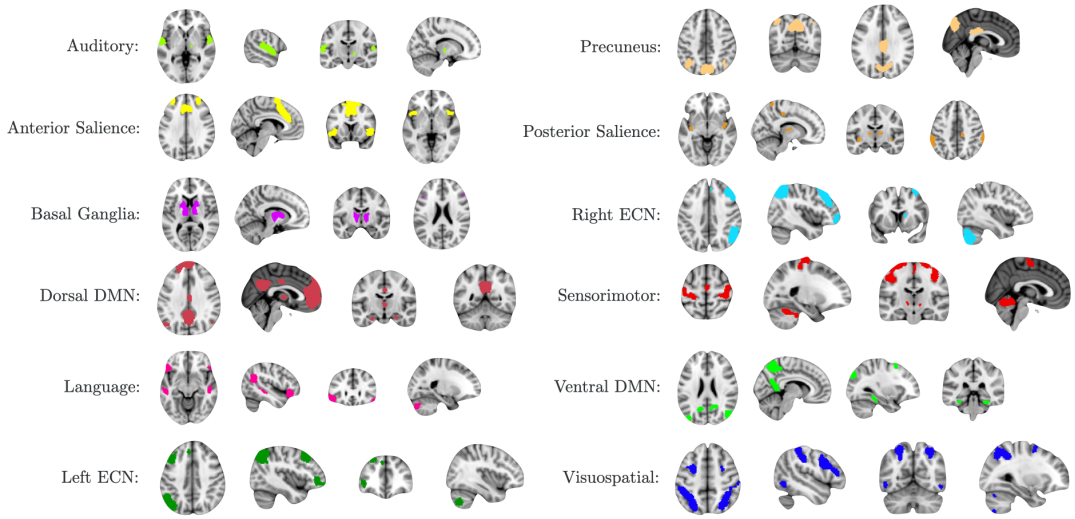

Figure 2.1: Shirer atlas functional brain networks [59]

as part of the preprocessing step.

A total of 12 distinct functional brain networks were analyzed in this study. Most of the highlighted results were from three networks: basal ganglia network (BGN), dorsal default mode network (DDMN), and left executive control network (LECN). As for the rest of the results, these are included in the appendices. The list of anatomical ROIs for all of the analyzed networks is summarized in Table A.2.

2.4 Pairwise maximum entropy model

To compare the brain dynamics of healthy and depressed participants, we implemented the Energy Landscape Analysis (ELA) method, which utilizes the P-MEM (Figure 2.2) [42]. In this study, ELA was conducted separately for each of the 12 distinct functional networks (see Table A.2).

In ELA, we began by combining the rs-fMRI data of all participants in the designated group (healthy and depressed) to create a group-level dynamics model.

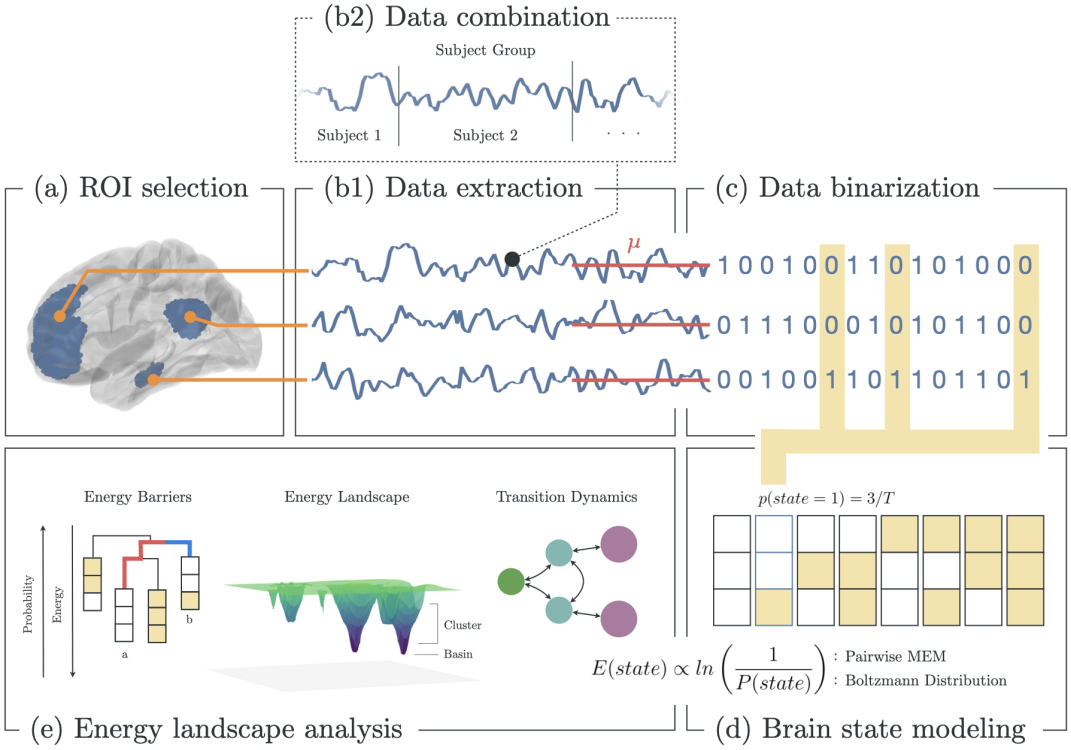

Figure 2.2: Methodology for energy landscape analysis

(a) Selection of ROI based on functional brain networks associated with depression. (b1) Extraction of fMRI BOLD signals from each ROI. (b2) All signals from participants in the designated group/s were combined. (c) Binarization of each signal using the mean BOLD value for each ROI. (d) Estimation of the state energy based on the emprical state frequency/probability. (e) Energy landscape analysis, including analyses of state energy levels, basin state landscape, and state transition dynamics. Note that as the energy of a state increases, its probability of occurrence decreases.

In the combined group, the concatenated time series data were extracted from the corresponding ROIs of the chosen functional network (Figure 2.2-a,b). ThenThen, the time series data were converted to binarized signals, using the average BOLD signal value through the entire timecourse data as the threshold (Figure 2.2-c). At any time point, binarized signals were either 1 (active, higher than or equal to the threshold) or 0 (inactive*, lower than the threshold). The threshold value

*The term *inactive* may be a misnomer since BOLD signals below the threshold do not necessarily imply inactivity. However, we are keeping this term to be consistent with previous studies.

was computed for each ROI across the combined data of the group participants. Despite the potential loss of information from converting a continuous time series into a binarized form, it has been shown that binarization does not eliminate important information on the functional interactions of brain regions [37, 45]. This binarization process is also performed to reduce the risk of overfitting the model [61].

Binarizing the signals allowed us to encode the time signals into brain state sequences, wherein a brain state was defined by the activity pattern, i.e., active and inactive ROIs, at a given time (Figure 2.2-c,d). An active ROI corresponds to the hemodynamic response correlated to the transient response of local field potentials (LFPs) at the said region [62, 63]. Given brain network with n ROIs, there are 2^n possible states. For each brain state σ, we computed the empirical probability $p(\sigma)$,

$$p(\sigma) = \frac{n_\sigma}{T} \tag{2.1}$$

where n_σ is the number of occurrences in which the state σ appeared in the time series, and T is the total length of the time series (Figure 2.2-d).

From the brain state probabilities, we defined the state energy using Boltzmann distribution [64]

$$P(\sigma|h, J) = \frac{\exp[-E(\sigma|h, J)]}{\sum_{\sigma'}[-E(\sigma'|h, J)]} \tag{2.2}$$

where the sum in denominator is taken over all 2^n possible states (each state is denoted by σ'). In P-MEM, the state energy $E(\sigma)$ in Equation 2.2 was restricted in the quadratic form, and expressed as:

$$E(\sigma|h, J) = -\sum_{i=1}^{n} h_i\sigma_i - \frac{1}{2}\sum_{i=1}^{n}\sum_{\substack{j=1 \\ j\neq i}}^{n} J_{i,j}\sigma_i\sigma_j \tag{2.3}$$

with $h = [h_i]_{i=1}^n$ and $J = [J_{i,j}]_{i,j=1}^n$ corresponding to the individual ROI activity and the pairwise ROI interaction, respectively. As implied by these equations, more active ROIs correspond to higher h and J, which leads to lower (more negative) energy (Equation 2.3), and higher occurrence probability (Equation 2.2) [42].

We then built the P-MEM from the model parameters h & J by maximizing their likelihood, as defined by:

$$(h, J) = \arg\max_{h,J} \mathcal{L}(h, J) \tag{2.4}$$

$$\mathcal{L}(h, J) = \prod_{t=1}^{T} P(\sigma(t)|h, J) \tag{2.5}$$

for the entire time series of length T.

Gradient ascent algorithm was performed to maximize the likelihood,

$$h_i^{new} - h_i^{old} = \frac{\epsilon}{T}\frac{\partial}{\partial h_i} log\mathcal{L}(h, J) \quad = \epsilon(\langle\sigma_i\rangle_e - \langle\sigma_i\rangle_m) \tag{2.6}$$

$$J_{i,j}^{new} - J_{i,j}^{old} = \frac{\epsilon}{T}\frac{\partial}{\partial J_{i,j}} log\mathcal{L}(h, J) = \epsilon(\langle\sigma_i\sigma_j\rangle_e - \langle\sigma_i\sigma_j\rangle_m) \tag{2.7}$$

where ϵ is the step size constant. The mean $\langle\sigma_i\rangle_e$ and pairwise correlation $\langle\sigma_i\sigma_j\rangle_e$ of the empirical data are computed as:

$$\langle\sigma_i\rangle_e = \frac{1}{T}\sum^{T} \sigma_i(t) \tag{2.8}$$

$$\langle\sigma_i\sigma_j\rangle_e = \frac{1}{T}\sum^{T} \sigma_i(t)\sigma_j(t) \tag{2.9}$$

while the mean $\langle\sigma_i\rangle_m$ and pairwise correlation $\langle\sigma_i\sigma_j\rangle_m$ of the model are computed as:

$$\langle\sigma_i\rangle_m = \sum_{k=1}^{2^n} \sigma_i P(\sigma^k) \tag{2.10}$$

$$\langle\sigma_i\sigma_j\rangle_m = \sum_{k=1}^{2^n} \sigma_i\sigma_j P(\sigma^k) \tag{2.11}$$

for all $k = 2^n$ states. Note that in Equations 2.8-2.9, $\sigma_i(t)$ denotes the ith ROI of the state at time t, while in Equations 2.10-2.11, σ^k denotes the state k [42, 43]. By using $\langle\sigma_i\rangle_e$ and $\langle\sigma_i\sigma_j\rangle_e$ as constraints, maximizing the entropy derives the state probability as a Boltzmann distribution (Equation 2.2) [46].

2.5 Energy landscape analysis

This study hypothesized that the depressive brain network operates differently than a healthy network and that ELA can capture such dynamics. With a singular pairwise model for healthy and depressed groups, we analyzed group-level energy landscape features, as well as individual-level transition dynamics (Figure 2.2-e). On the group level, we identified the basin states for each network. Basins are the core unit of ELA. By defining basins as states with local minimum energy [65], we can observe how the brain system transitions among these relatively stable states [45]. These dynamics may be in terms of network stability (basin occurrence frequency), network efficiency (traveling/ease-of-transition score [43]), or network concentration (lingering score). The ELA features analyzed in this study are summarized in Table 2.3.

At the beginning of ELA, basin state dendrograms were constructed by finding the basin states and their clusters. Basin states (or basins) have the lowest energy relative to their neighboring states. States are neighbors if they differ in only one active/inactive region. If neighboring states have lower energy barriers than other states, they become part of the closest basin cluster [43]. Basins are the core of energy landscapes since these states are presumed to be the most stable. Djikstra's algorithm was performed to search for the basins and construct the leaves (basins) and branches (energy barriers) of the dendrogram. Figure 2.2-e: *Energy Barriers* highlights the energy barrier between states a and b (red: $a \rightarrow b$; blue: $b \rightarrow a$). Here, $a \rightarrow b$ has a higher barrier, and thus has a lower probability of occurring [43].

Energy landscapes were then constructed to depict the basins' energy level and cluster size. In Figure 2.2-e: *Energy Landscape Analysis*, a 3D schematic diagram depicts the basins in arbitrary state space. Here, basin clusters are plotted as concentric circles, where the basin is at the center, and neighboring states are on circles with a radius equivalent to their distance to the basin (i.e., a state that differs in one region with the basin has a distance of 1, state the differs in two regions has a distance of 2, and so on). Thus each circle represented the states

Table 2.3: Energy landscape features

Level	Feature	Description	
Group	Basin	States with the lowest energy relative to neighbors	Fig. 3.3, Fig. 5.2, Fig. 3.2, Fig. 4.2, Fig. 5.3
	Major basin	Two basins with the lowest energy	Fig. 3.3, Fig. 5.2, Table B.2, Table C.2, Table D.2
	Minor basin	Non-major basin	Fig. 3.3, Fig. 5.2, Table B.2, Table C.2, Table D.2
	Basin size	Number of neighboring states clustered to a basin	Fig. 3.2, Fig. 4.2, Fig. 5.3, Table B.2, Table C.2, Table D.2
	Basin energy	Energy level of a basin	Eq. 2.3, Fig. 3.3, Fig. 5.2, Table B.2, Table C.2, Table D.2
Individual	Basin occurrence frequency	Number of times the basin occurred in an individual participant's fMRI time series data	Fig. 3.4, Fig. 4.3, Fig. 5.4, Table B.1, Table C.1, Table D.1
	Traveling score	Rate of successful transition from one major basin to another	Eq. 2.16, Fig. 3.5, Fig. 4.4, Fig. 5.5, Table B.3, Table C.3, Table D.3
	Lingering score	Rate of staying within each of the major basins, or their peripheral (clustered) states	Eq. 2.17, Fig. 3.5, Fig. 4.4, Fig. 5.5, Table B.3, Table C.3, Table D.3

that were equidistant to the basin. Then for each circle (including the center), its depth was equivalent to the state's energy with the lowest energy (Equation 2.3) in that circle.

Since energy landscapes modeled only the group-level brain dynamics, we also analyzed the brain dynamics of individual participants by computing the occurrence frequency of basins $f(A)$ on individual fMRI time series. The occurrence frequencies of all basins (major and minor) are then summed for each group and each network.

For each network, we selected two major basins, A_1 and A_2, as the basins

having the lowest energy, with P_1 as clustered states for A_1, P_2 for A_2. Then we computed the following participant-level transition rates,

$$TR(A \to A') = \frac{n(A_1 \to A_2) + n(A_2 \to A_1)}{T} \tag{2.12}$$

$$TR(P \to P') = \frac{n(P_1 \to P_2) + n(P_2 \to P_1)}{T} \tag{2.13}$$

where $n(U \to V)$ is the number of times the participant's time series entered state U and arrived at state V; $TR(A \to A')$ is the major transition rate for major basins; $TR(P \to P')$ is the peripheral transition rate for clusters of major basins. Moreover, we computed the staying rates of the states,

$$SR(A \to A') = \frac{n(A_1 \to A_1) + n(A_2 \to A_2)}{T} \tag{2.14}$$

$$SR(P \to P') = \frac{n(P_1 \to P_1) + n(P_2 \to P_2)}{T} \tag{2.15}$$

where this time we counted the number of times the participant's brain activity stayed on the major basins ($SR(A \to A')$), or the periphery ($SR(P \to P')$). The transition rates were used to define the *Traveling Score*, which measured the amount of times the brain successfully *traveled* from one major basin to another (Equation 2.16, Figure 3.5-a). Similarly, the staying rates were used to define the *Lingering Score*, which measured the amount of times the brain *lingered* on a basin or along its periphery (Equation 2.17, Figure 3.5-a),

$$Traveling\ Score = \frac{TR(A \to A')}{TR(P \to P')} \tag{2.16}$$

$$Lingering\ Score = SR(A \to A') + SR(P \to P') \tag{2.17}$$

Note that the traveling score (Equation 2.16) is also known as efficiency score, based on the ease of transitions index [43].

2.6 Statistical tests

Wilcoxon-Mann-Whitney was performed to find significant group differences (healthy vs. group) in participants' age, IQ, BDI-II, and SHAPS (Snaith-Hamilton Pleasure Scale) scores. Similarly, Chi-squared test was performed for group differences

in sex. Group differences are presumed to be statistically significant at $p < 0.05$ for both types of statistical analyses. One-way ANOVA with Bonferroni correction was applied to test for statistical significance of results when comparing individual- and group-level differences in energy landscape characteristics such as major basin frequency and transition rates. These results were also verified by Kruskal-Wallis test to cope with non-normally distributed data.

3 Singular Model for Depression Biomarker

The characterization of neural dynamics can uncover good candidates for depression biomarkers. Several studies have proven that MDD results from dysfunctional brain processes [2, 16, 17, 19–21, 30–32, 34]. These processes include (but are not limited to): mood regulation [19–21, 30, 32], emotional processing [16, 17, 30–32, 34], reward anticipation [16, 17, 32], pain recognition [17, 30], self-referential thoughts [30–32, 34], and attention control [30–32, 34]. Moreover, a recurring theme among depression studies paints MDD as a stuck state [2, 47, 48]. This evidence highly suggests that impairment in neural circuitry prevents the depressed brain from functioning normally. Moreover, we analyzed the neural dynamics of depressed patients using the ELA framework for these reasons.

3.1 Conceptual framework

When designing the model framework, one crucial consideration has been building a singular model for healthy and depressed groups. Ideally, a singular model would approximate the "general" individual, an individual who—regardless of age, sex, and even IQ—may or may not have MDD. This model can then compare the actual healthy and depressed individuals, measure their differences, and classify one from another (Figure 3.1).

In contrast, a separate model framework would build different models out of the two groups. These models can be compared directly, without the additional process of applying the model to individual data. Having a separate model for depression, specifically MDD, would be beneficial in the long run if we consider using the same framework to develop models for other mental disorders. Such a

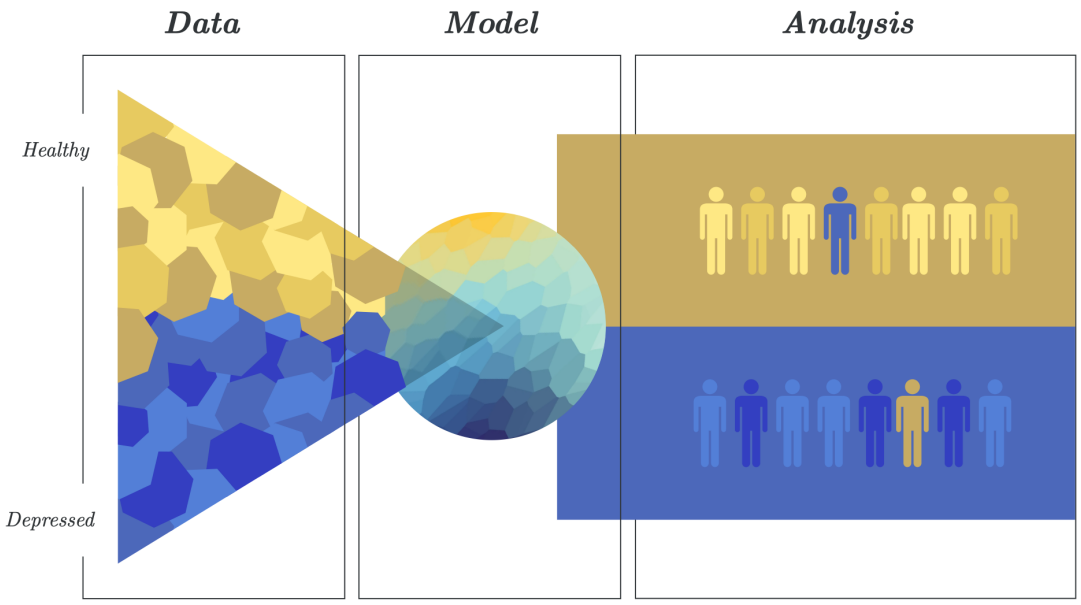

Figure 3.1: Singular model: Energy landscape framework
Data from healthy and depressed participants are combined to create a singular model. This model is used to distinguish between healthy and depressed individuals, which may be used as potential biomarker for depression.

collection of mental disorder models may help demarcate the boundaries between each mental disorder, thus improving diagnosis and specialized treatment.

Nevertheless, our decision to build a singular model is influenced by our primary goal of discovering biomarkers. Biomarkers are objective measurements of biological, pathogenic, or pharmacological processes that indicate the presence of a disease or disorder [66]. Substitution to a clinical endpoint is a mark of a successful biomarker [66]. Thus, it is essential to note that the role of a biomarker is to measure the effects of treatment primarily and only to help understand the disorder secondarily. With a singular model, we can create a baseline for the "general" individual, which acts as a measuring tool for evaluating the neural activity features of MDD. These features can then be correlated with certain types and degrees of treatment. On the other hand, a separate model framework replaces this baseline with the healthy group model, which may be riddled with bias depending on the selection criteria used for determining a "healthy" individual.

We conducted two levels of analysis in this study (Table 2.3). On the group

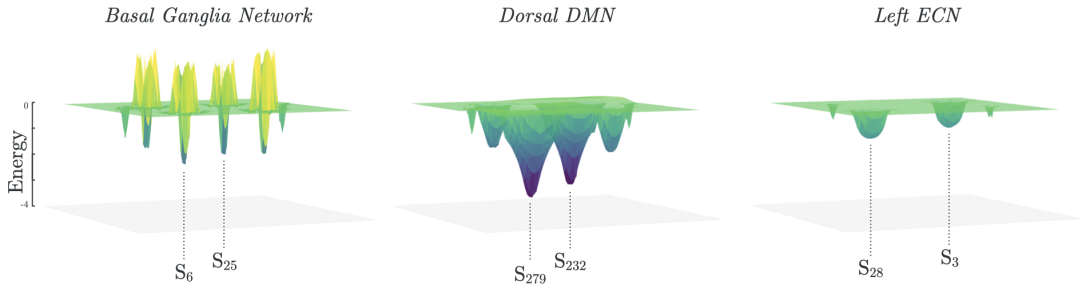

Figure 3.2: Separate model: Energy landscapes

3D visualization of the energy landscapes from combined data of healthy and depressed groups on BGN, DDMN, and LECN. Major basin states on each network are indicated.

level, features such as basins (major and minor), basin size, and basin energy were shared by individuals in the model. On the individual level, specific neurodynamic features of individuals such as basin occurrence frequency, dynamic traveling, and lingering scores were measured.

3.2 Energy landscape

From the combined data of healthy and depressed individuals, we constructed the energy landscapes for each functional brain network, as previewed in Figure 3.2. These energy landscapes confirmed that the brain at rest is a multi-stable state system [46]. The basin characteristics of the energy landscapes on all networks are summarized in Table B.2 and visualized in Figure B.1. Some networks such as DDMN have prominent major basins (i.e., major basins with high energy barrier/difference compared to minor basins). In contrast, other networks such as PSN seem to have less prominent major basins. Moreover, the number of basins may be attributed to the number of ROIs in the network, with AN having the least number of basins (2 basins, 3 ROIs) and PSN having the most basins (11 basins, 10 ROIs). This pattern is not consistent, though, as PN (6 basins, 4 ROIs) has more basins than LECN (4 basins, 5 ROIs) despite having fewer ROIs.

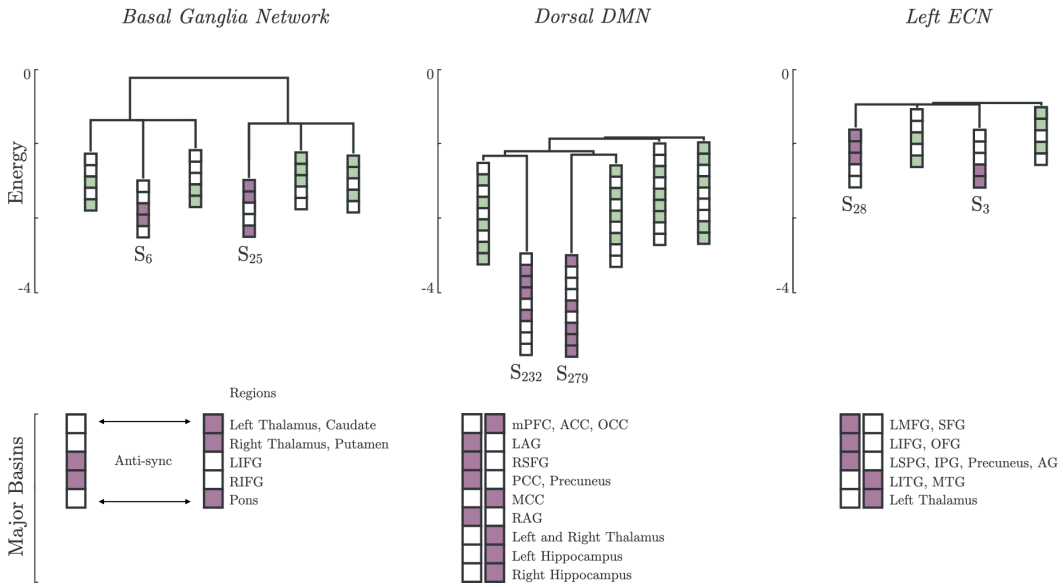

Figure 3.3: Singular model: Major and minor basins

Major basin states (purple) and minor basin states (green) from combined healthy and depressed groups on BGN, DDMN, and LECN. For each state, colored boxes correspond to activated regions, and white boxes to inactive regions.

3.3 Basins and activated regions

One of the novelties of our model is its capability to show network-wide interactions of all regions, whereas FCA-based models are limited to pairwise interactions only. In Figure 3.3, we can observe which regions had synchronous activations based on the model's stable states (major and minor basins). We define *synchronous activity* patterns between ROIs as being activated together in a major basin state [43]. The synchronous activity of different brain regions may be associated with coherent oscillations, suggesting high functional connectivity in them [67]. On the other hand, anti-synchronicity, in the context of our analysis, could reveal either functional disconnectivity (i.e., regions do not activate together) or negative functional connectivity (i.e., regions activate contrarily) [68].

The first observable pattern from these results was the synchronized activities

of left and right regions within the same network. In BGN, all stable states (major and minor basins) had synchronous activation/inactivation of the left and right thalamus regions; and similarly in the left and right inferior frontal gyrus (LIFG, RIFG) over the major basins. In DDMN, the left and right hippocampus were synchronized across all basins, while the left and right angular gyrus (LAG, RAG) were synchronized over the major basins. These patterns may suggest a strong coupling in super regions (e.g., thalamus and hippocampus) that have been separated into left and right subregions by the ROI selection method performed beforehand (see Section 2.3).

Another recurring pattern across networks was the anti-synchronicity of major basins. Major basins were selected based on the energy level of each state (see Section 2.5) and, in principle, describe the most probable states that the brain will enter at rest. In Figure 3.3, under BGN, we can see two major basins, one with regions LIFG and RIFG activated and another with the left and right thalamus, caudate, putamen, and pons regions activated. These two states have opposing activations, which suggests that the brain at rest alternates in switching these functionally-correlated regions on and off. This pattern of anti-synchronous major basins was also present in DDMN, LECN (Figure 3.3), and the rest of the networks analyzed in this study (Table B.2).

3.4 Transition dynamics

We applied the model to individual participant data to analyze the brain dynamics patterns between healthy and depressed groups. First, we investigated the occurrence frequency of major basins for each group across the 12 networks (Figure 3.4, Table B.1). In ASN, the healthy group had a slightly higher visiting occurrence of the major basins than the depressed group ($\bar{f}_{Healthy} = 0.2819$, $\bar{f}_{Depressed} = 0.2798$). The opposite was true for other regions such as AN ($\bar{f}_{Healthy} = 0.6352$, $\bar{f}_{Depressed} = 0.6409$) and SMN ($\bar{f}_{Healthy} = 0.43819$, $\bar{f}_{Depressed} = 0.4448$). However, upon testing for group differences using one-way ANOVA, none of the results were statistically significant.

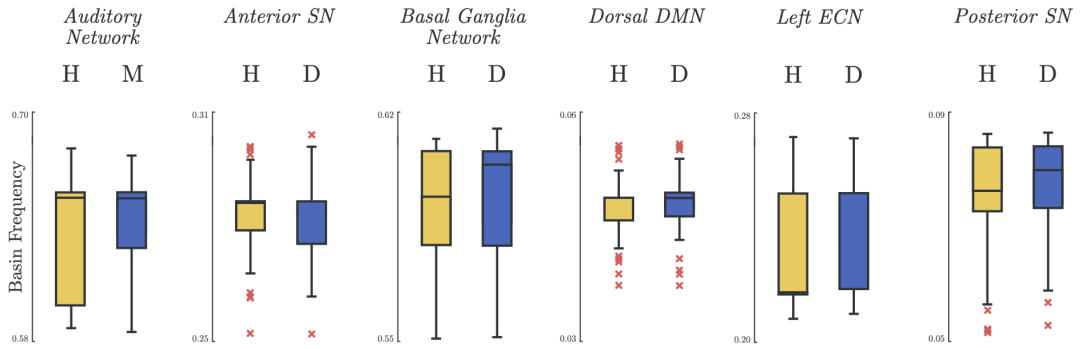

Figure 3.4: Singular model: Basin occurrence frequency

Occurrence frequency of basins for healthy and depressed groups on various brain networks. No significant differences were found between groups using one-way ANOVA (see Table B.1).

Next, we investigated individual transition dynamics based on two dynamics scores. The traveling score captures the brain's attraction to oscillate between the two major basins. It measures the ease of transition in neural dynamics necessary for executive processes, which correlates to performance scores on neuropsychological tests for verbal and non-verbal executive functions [43]. In both healthy and depressed groups, there were higher traveling scores ($Traveling\ Score > 0.5$) on AN, BGN, and PN; as compared to low-scoring networks such as DDMN, LN, LECN, PSN, VDMN and VSPN (Figure 3.5, Table B.3).

On the other hand, higher lingering scores ($Lingering\ Score > 0.5$) were observed in DDMN, LECN, and SMN, whereas BGN, PSN and VSPN scored low. While traveling score attempted to measure the dynamic activity of the brain, the lingering score was formulated to measure the concentrated neural activity, which may shed light on repeating though patterns such as rumination. Unfortunately, similar to the results on major basin frequency, there were no significant differences between the healthy and depressed groups on individuals' traveling and lingering scores.

These underwhelming results led us to rethink our model framework. In the next section, we discuss the changes we made and their implications in detail.

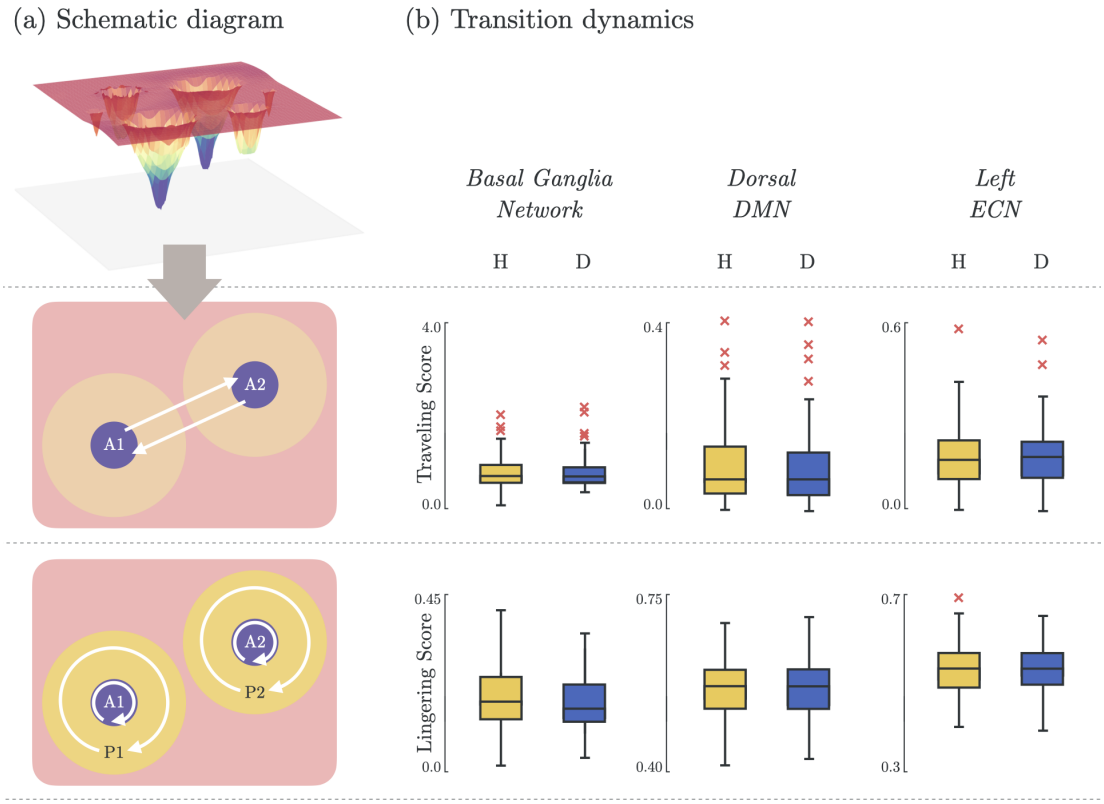

Figure 3.5: Singular model: Transition dynamics

(a) Schematic diagram illustrating the transition dynamics for traveling score (basin-to-basin; Equation 2.16) and lingering score (within-basin or within-peripheral; Equation 2.17). (b) Traveling and lingering scores for healthy and depressed groups on BGN, DDMN, and LECN.

4 Separate Model for Major Depression

In our initial efforts to discover biomarkers for depression, we developed an energy landscape model to analyze the brain dynamics of individuals diagnosed with MDD. However, the results have been inconclusive. One possible culprit is heterogeneity in the data [14, 16–21]. As we discussed in Section 1.1, depression biomarkers are potential solutions to the confounding effects of heterogeneity partly caused by the symptoms-based classification of MDD. Since our participants were diagnosed using the system mentioned above, the heterogeneous aspects of the data may have been absorbed by the model as well. Counter to this point, some of the individual-level analyses results seem to suggest that the depressed group is "less heterogeneous" (or more homogeneous) than the healthy group since there was lower variance among the depressed individuals (see Figures 3.4 and 3.5).

Our model framework itself may be another possible cause for failing to reveal characterizing neurodynamic features of MDD. In the past, P-MEM and ELA have been successfully used to differentiate network-scale dynamical changes across different age groups [43] and individuals with autism spectrum disorder (ASD) [61]. In both studies, separate ELA models were built for each group (young vs. old [44]; typically developing vs. ASD [61]). These contrast our initial singular model framework.

4.1 Separate framework

From what we have learned in the previous chapter, discovering biomarkers for MDD using our initial model framework was more challenging than anticipated.

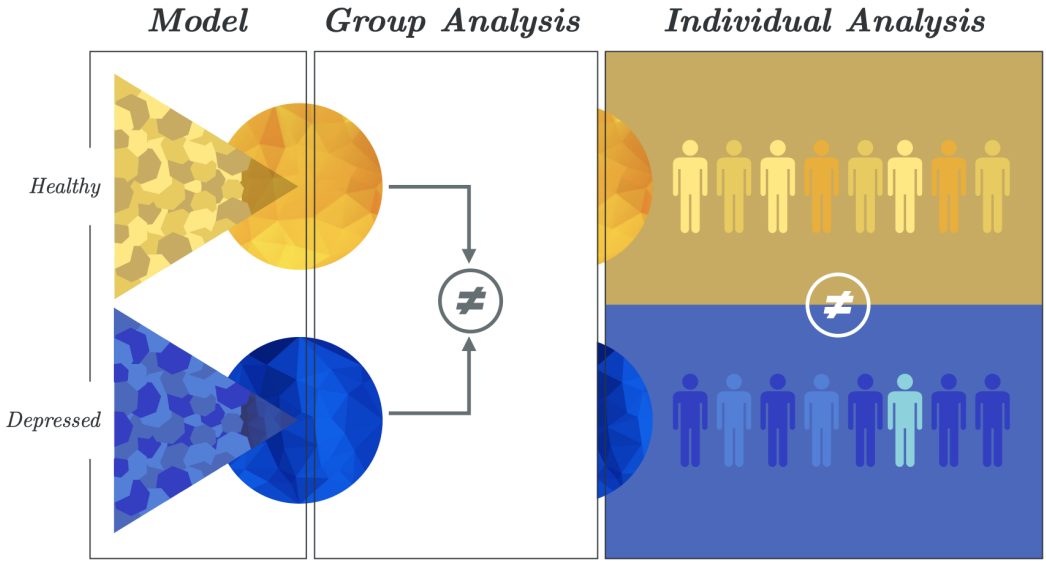

Figure 4.1: Separate model: Conceptual framework
Two separate models were created from healthy and depressed groups. With these models, group-level and individual/participant-level comparisons can distinguish between the groups.

In response, we designed a new framework that is more grounded on existing literature [42, 43, 45, 46, 61]. With our new framework (Figure 4.1), we fitted separate pairwise MEMs on the healthy and depressed groups. In turn, this framework allowed us to compare the groups on the individual and group levels.

4.2 Energy landscapes

Two energy landscapes were constructed from the separate model framework. In some networks, there was a stark difference in these landscapes. For example, in DDMN, the singular model found six basins, while the separate model found five basins for the healthy and seven basins for the depressed group, as shown in Figure 4.2. However, the major basins (S_{232}, S_{279}) remained the same for both models and groups. In other networks, the energy landscapes were similar across models and groups. This pattern was evident in BGN, where the basins were con-

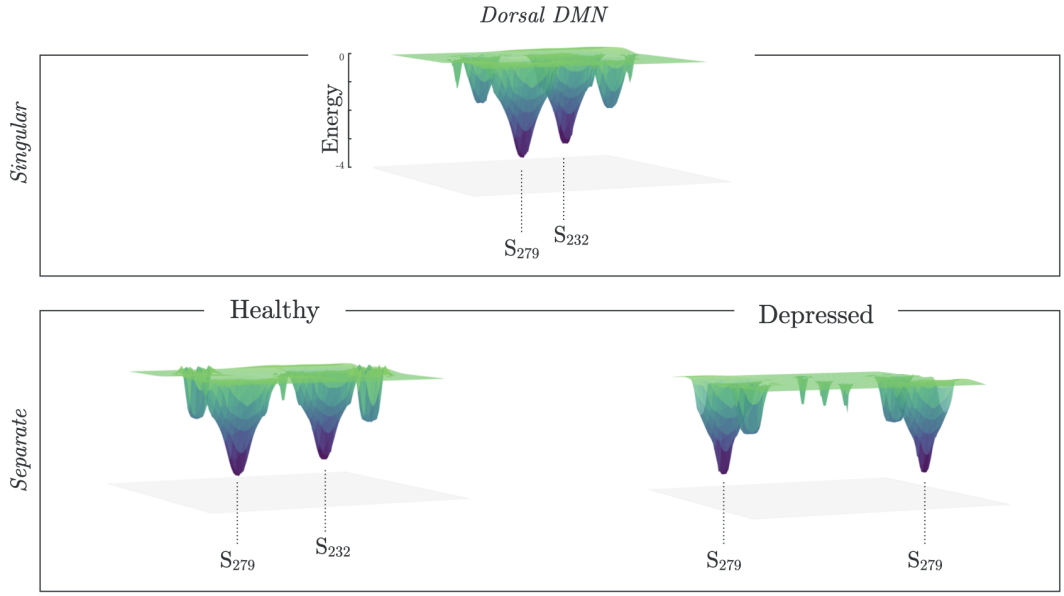

Figure 4.2: Separate model: Energy landscapes

Comparison of energy landscapes for singular and separate models for healthy and depressed groups on DDMN. (Table C.2).

sistent (major: S_6, S_{25}; minor: S_3, S_5, S_{26}, S_{28}). However, the energy and size of these basins differed (e.g., singular: $E(S_6) = -1.96, size(S_6) = 25.00\%$, healthy: $E(S_6) = -1.92, size(S_6) = 25.00\%$, depressed: $E(S_6) = -2.01, size(S_6) = 28.12\%$). For a full comparison, see Tables B.2 and C.2.

4.3 Basin frequency

We then tested for statistical group differences in the major basin frequencies of individual participants in the healthy and depressed groups. With the separate model framework, we were able to find significant differences across all networks using one-way ANOVA and Kruskal-Wallis test (see Table C.1). We can observe such differences in Figure 4.3, where the healthy group operated on a different frequency than the depressed group in each network. Compared to the single model results in Figure 3.4, constructing separate models can have more discrim-

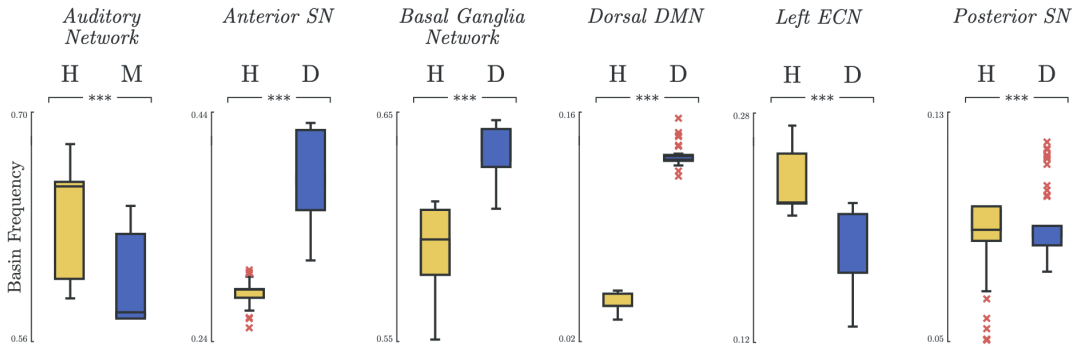

Figure 4.3: Separate model: Major basin frequency

Occurrence frequency of basins for healthy and depressed groups on various brain networks. (***) $p < 0.005$; between-group comparison of basin frequencies using one-way ANOVA and Kruskal-Wallis test (except for PSN, which had no significant difference in Kruskal-Wallis test).

inative power over healthy and depressed groups. See Table C.1 for the complete results.

4.4 Transition dynamics

More significant differences were found in the separate model framework when we analyzed the transition dynamics of both groups. In terms of lingering scores, there were group differences on networks such as DDMN and LECN (as shown in Figure 4.4), LN, RECN, VDMN, and VSPN. As for traveling scores, only RECN also showed a significant difference. There were other significant results found in traveling rates for basin clusters ($TR(P)$: DDMN, LN, LECN, PSN, RECN, VDMN, VSPN), staying rates for major basin ($SR(A)$: ASN, PSN, SMN), and staying rates for basin clusters ($SR(P)$: ASN, DDMN, LN, LECN, PN, RECN, SMN, VDMN, VSPN). Among the networks, AN and BGN had no significant results in transition dynamics metrics (Table C.3). Nevertheless, such differences were not present in the single model, as shown in Figure 3.5.

We achieved significant results that answered our question, *"does the depres-*

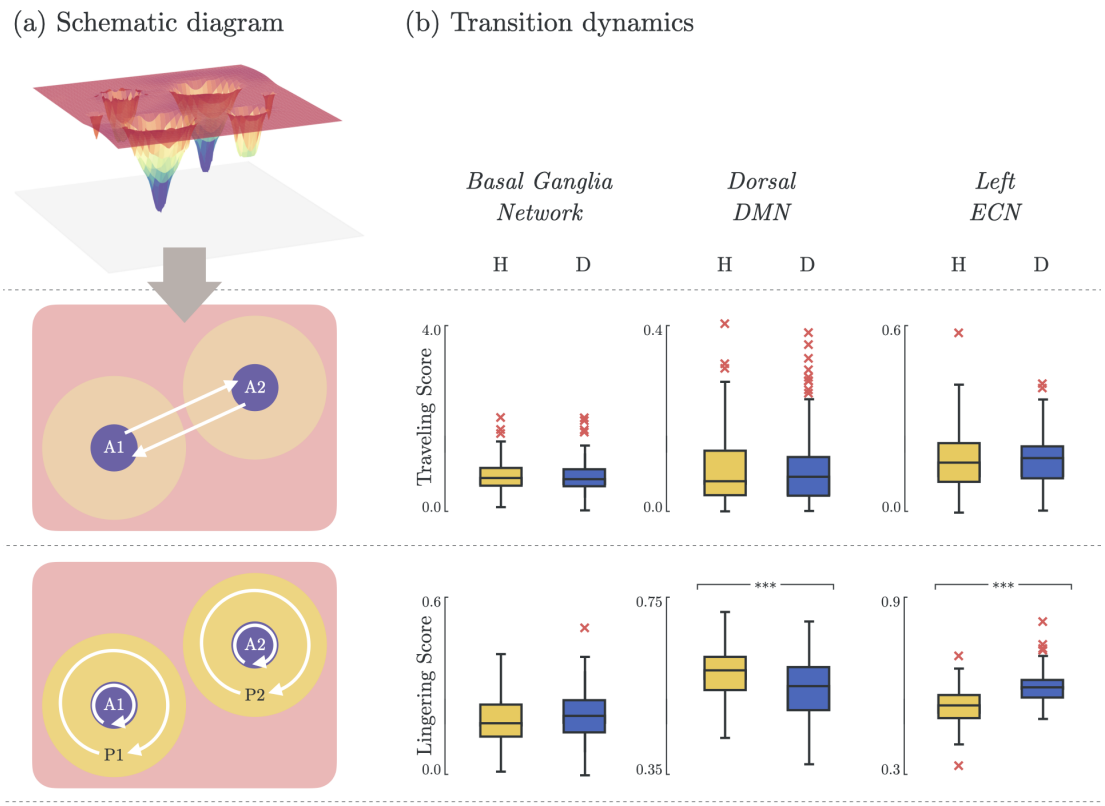

Figure 4.4: Separate model: Transition dynamics

(a) Schematic diagram illustrating the transition dynamics for traveling score (basin-to-basin; Equation 2.16) and lingering score (within-basin or within-peripheral; Equation 2.17). (b) Traveling and lingering scores for healthy and depressed groups on BGN, DDMN, and LECN.

(***) $p < 0.005$; traveling/lingering scores group comparison using one-way ANOVA.

sive brain network have distinct brain dynamics?" However, this led us to another question, *"if major depression is heterogeneous in nature, would its homogeneous subgroups have distinct energy landscapes as well?"*. In the next section, we discuss our investigative efforts towards analyzing the energy landscapes of a particular subtype of major depressive disorder known as melancholic depression.

5 Segregated Model for Melancholic Depression

Depression and melancholia are synonymous terms in ordinary speech but have different technical meanings in psychiatry [69]. Chapter 1 gives an overview of how the term *depression* evolved and detached from *melancholia* in the clinical sense. While depression is associated with "deepened or prolonged sadness in everyday life," melancholia is predominantly marked by "loss of pleasure or interest" (or anhedonia), along with many other depressive symptoms [69, 70]. In DSM-V, melancholia is regarded as a feature for depression and other mental disorders [10]. Despite the pressing evidence for melancholic depression to be considered a distinct subtype of depression, it has unfortunately been overshadowed by the focus of most research on major depression [70–72].

Nevertheless, there has been a significant thrust on classifying melancholic depression, as this subtype of depression has been deemed to be more severe than its non-melancholic counterpart [73–75]. Researchers have focused on distinguishing the two because of the overlapping symptoms between depression and melancholia. This distinction is essential for both diagnosis and treatment since melancholic patients (i.e., MDD with melancholic features) may have different responses to treatment [70]. For example, they respond better to tricyclic antidepressants (TCAs) than to selective serotonin reuptake inhibitors (SSRIs) [76]. On the contrary, they do not respond well with psychotherapy and placebo compared to non-melancholic patients [77]. Thus clearly, a correct diagnosis of melancholic depression is the next step towards better treatment.

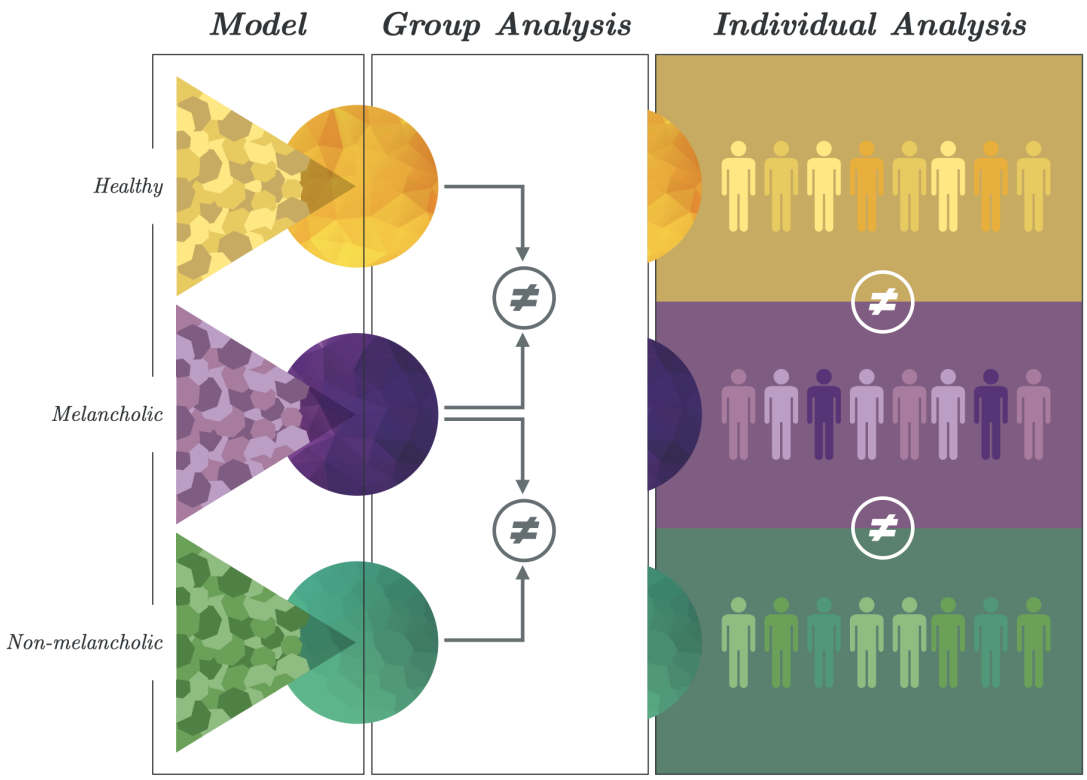

Figure 5.1: Segregated model: Conceptual framework

Three separate models were created from each group: healthy, melancholic, and non-melancholic. With these models, group-level and individual/participant-level comparisons can distinguish melancholic depression from the other groups.

5.1 Segregated framework

We adapted our separate model framework in the previous section to explore the energy landscapes of the melancholic depression subtype. Our new framework comprised segregated models for three groups: healthy, non-melancholic, and melancholic depression. As depicted in Figure 5.1, this framework allowed the group and individual levels to be analyzed. We hypothesized that, due to depression heterogeneity, the energy landscapes of the melancholic group would be different not only to the healthy group but also to the non-melancholic group. The latter distinction would solidify our presumption that the original framework failed because of heterogeneity in the depression data.

Table 5.1: Updated demographic data for melancholic and non-melancholic subgroups

		Depressed		
	Healthy	Non-Melancholic	Melancholic	P-value
No. of participants	142	31	89	
Sex (female / male)[1]	71 / 71	16 / 15	44 / 45	
Age (years)[2]	42.62 ± 14.33	41.48 ± 9.46	43.37 ± 11.65	
BDI-II[2]	5.34 ± 3.76	29.13 ± 6.08	32.40 ± 7.88	(∗)(∗∗∗)
Anhedonia (SHAPS)[2]	23.27 ± 6.20	34.21 ± 5.30	37.72 ± 6.22	(∗)(∗∗∗)
IQ (JART)[2]	110.92 ± 8.813	114.09 ± 9.57	111.61 ± 9.30	
Site participants (HUH/HRC/HKH/COI)[1]	44 / 32 / 20 / 46	10 / 6 / 7 / 8	48 / 7 / 13 / 21	(∗∗)
Time samples per participant	161.90 ± 45.51	156.68 ± 50.34	155.39 ± 40.89	

BDI-II, Beck Depression Inventory-II; SHAPS, Snaith-Hamilton Pleasure Scale; JART, Japanese Adult Reading Test
Recruitment sites: Hiroshima University Hospital (HUH), Hiroshima Rehabilitation Center (HRC), Hiroshima Kajikawa Hospital (HKH), Center of Innovation in Hiroshima University (COI)

[1] Multiple group comparison using pairwise Chi-squared tests
[2] Multiple group comparison using one-way ANOVA with Bonferroni correction

(∗) $p < 0.05$ between non-melancholic and melancholic groups
(∗∗) $p < 0.01$ between healthy and melancholic groups
(∗∗∗) $p < 0.005$ between healthy and non-melancholic groups, and between healthy and melancholic groups

With the new framework, depressed participants were categorized into the melancholic group if they exhibited melancholic features based on the MINI interview (DSM-IV criteria) [51]. Otherwise, they are categorized into the non-melancholic group. As a result, there were 89 melancholic (44 F / 45 M) and 31 non-melancholic (16 F / 15 M) participants. Table 5.1 reflects the updated data set. The distribution of participants across sex, age, and IQ remained insignificant ($p > 0.05$, $healthy(H)$ vs. $non-melancholic(N)$ vs. $melancholic(M)$, multiple comparison tests). Similarly, there were significant differences in BDI-II and SHAPS scores ($p < 0.005$, H vs. N, H vs. M), as well as distribution of participants across fMRI recording sites ($p < 0.01$, H vs. M). It is also important to note that the melancholic group scored significantly higher in depression severity (BDI-II) and anhedonia (SHAPS) than the non-melancholic group ($p < 0.05$, N vs. M).

5.2 Basins and energy levels

The basin dendrograms of each group across networks revealed differences in major basins and energy levels, as shown in Figure 5.2. In both BGN and LECN,

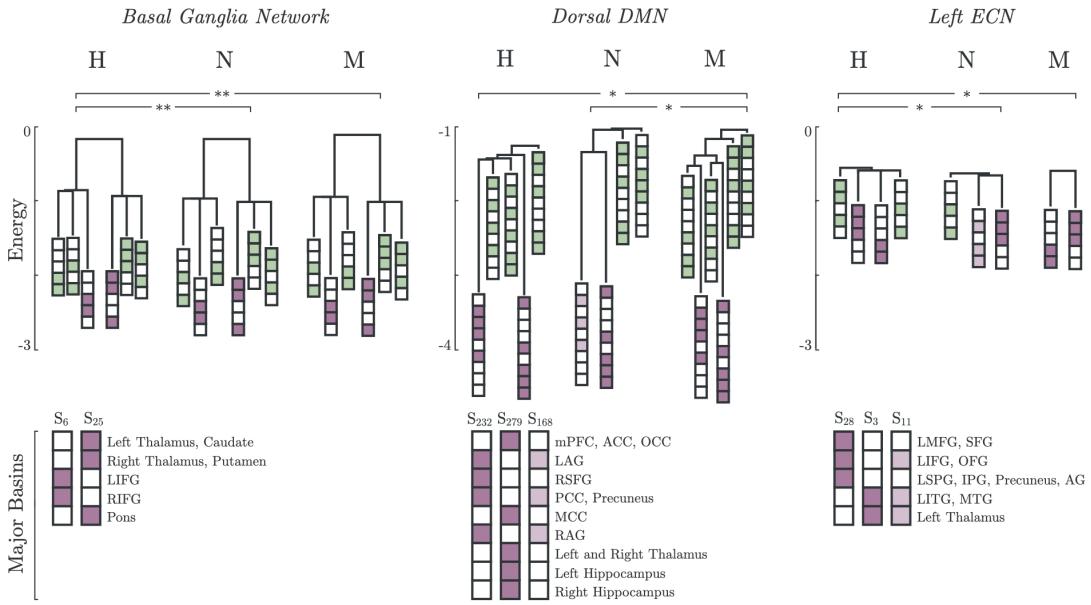

Figure 5.2: Segregated model: Major and minor basins

Major basin states (purple) and minor basin states (green) for healthy, non-melancholic, and melancholic groups on BGN, DDMN, and LECN. For each state, colored boxes correspond to active regions, and white boxes to inactive regions. Energies of the deepest major basins for each group are also indicated (see Table D.2 for summary of all major basin energies).

the non-melancholic and melancholic groups had deeper (i.e., lower energy) major basins than the healthy group. Remarkably, a different pattern can be observed in the DDMN, where the major basins of the non-melancholic group were shallower (i.e., higher energy) than those of the healthy and melancholic groups.

Furthermore, some major basins were unique to specific groups. For example, the non-melancholic group had a unique major basin in DDMN, where the left and right angular gyri (LAG, RAG), posterior cingulate cortex (PCC), and precuneus regions were activated. Similarly, on LECN, the non-melancholic group also had a unique major basin, where the left inferior frontal gyrus (LIFG), orbitofrontal gyrus (OFG), left inferior temporal gyrus (LITG), middle temporal gyrus (MTG), and left thalamus regions were activated. Complete results for basins and their energy levels are reported in Table D.2.

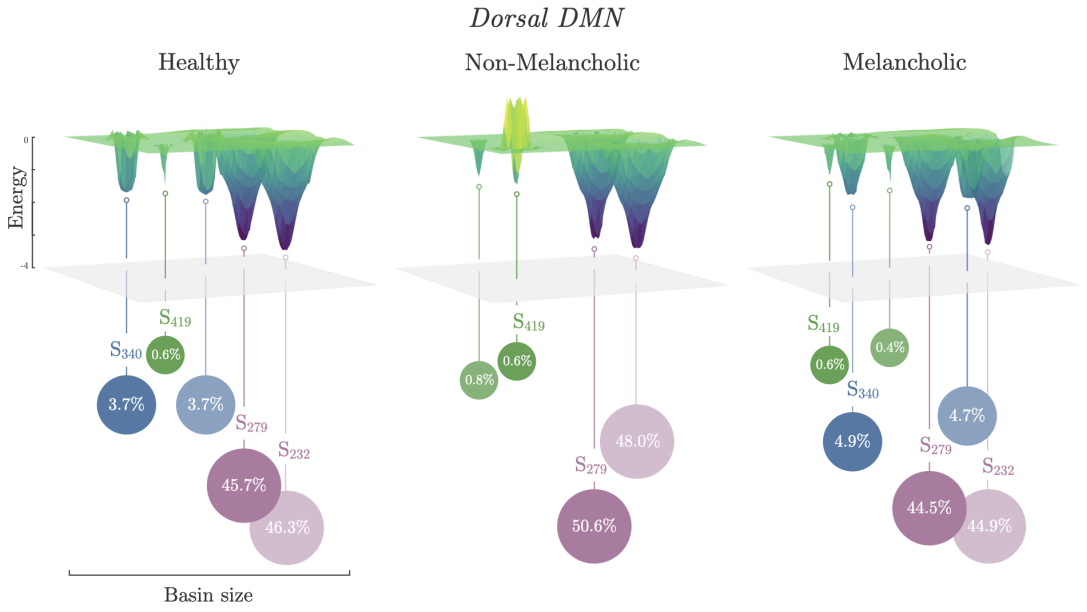

Figure 5.3: Segregated model: Energy landscapes

3D visualization of energy landscapes for healthy, non-melancholic, and nelancholic groups on DDMN. States are clustered to the their nearest basin state (Section 2.5). States S_{279} and S_{232} are the common major basins among the groups, while S_{340} and S_{419} are the common minor basins (Table D.2).

5.3 Energy landscapes

Energy landscapes were then constructed based on the basin information. As shown in Figure 5.3, each group had unique energy landscapes for DDMN. The melancholic group had the most number of basins ($n = 6$), followed by the healthy group ($n = 5$), then the non-melancholic group ($n = 4$). Among the energy landscapes for the 12 networks, DDMN had the only instance where the melancholic group had more basins than the other groups. Having more basins may suggest a busier network. On the other hand, the non-melancholic group had relatively larger major basins ($size_{A_1,A_2} = 98.6\%$), compared to the healthy ($size_{A_1,A_2} = 92.0\%$) and melancholic groups ($size_{A_1,A_2} = 89.4\%$). This result is natural for having fewer basins. Although a lower basin count may imply higher network stability, the *hill* cluster (B_2) of the non-melancholic group would suggest otherwise (see Table D.2 and Figure D.1 for summary of basin sizes).

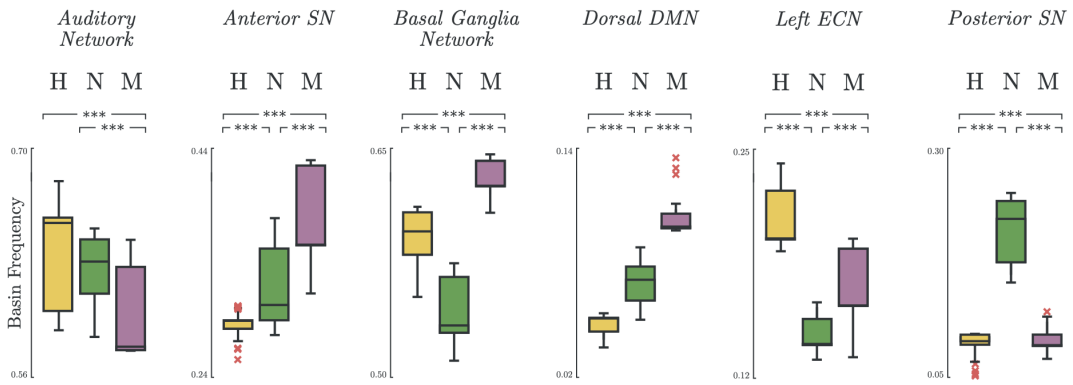

Figure 5.4: Segregated model: Major basin frequency

Occurrence frequency of basins for healthy, non-melancholic, and melancholic groups on various brain networks. (***) $p < 0.005$; between-group, pairwise comparison of basin frequencies using one-way ANOVA with Bonferroni correction

5.4 Basin frequency

Unlike the results in our previous framework, significant group differences were found on the individual basin frequencies when analyzed for all networks. The most notable results are summarized in Figure 5.4. There was a natural decreasing trend from healthy to melancholic groups in some networks (e.g., $p < 0.005$; *H vs. M*, *N vs. M*; *Auditory Network*). An opposite, increasing trend appeared in other networks (e.g., $p < 0.005$; *H vs. N*, *H vs. M*, *N vs. M*; *Anterior Salience Network*, *DDMN*). Finally, for the rest, the non-melancholic group had either the lowest (e.g., $p < 0.005$; *H vs. N*, *H vs. M*, *N vs. M*; *BGN*, *LECN*) or highest frequency (e.g., $p < 0.005$; *H vs. N*, *H vs. M*, *N vs. M*; *Posterior Salience Network*). Similar results for the other functional networks are listed in Table D.1.

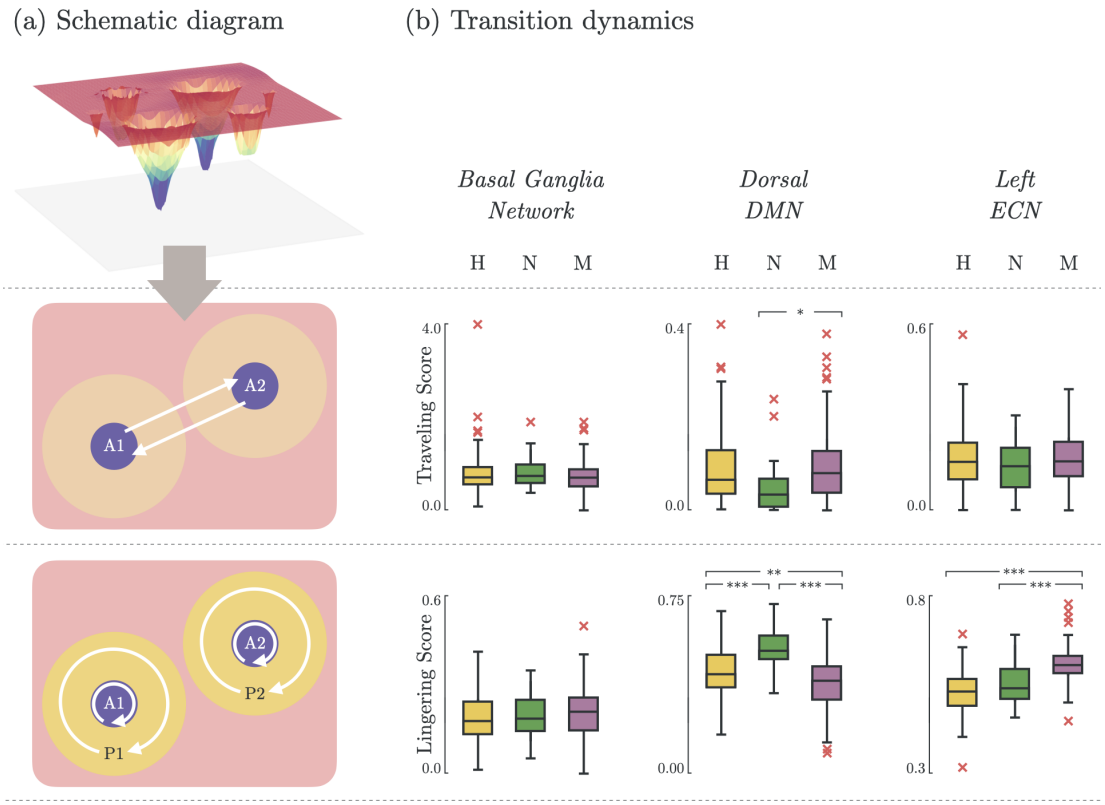

Figure 5.5: Segregated model: Transition dynamics

(a) Schematic diagram illustrating the transition dynamics for traveling score (basin-to-basin; Equation 2.16) and lingering score (within-basin or within-peripheral; Equation 2.17). (b) Traveling and lingering scores for healthy, non-melancholic, and melancholic groups on BGN, DDMN, and LECN.
$(*)$ $p < 0.05$; $(**)$ $p < 0.01$; $(***)$ $p < 0.005$; between-group, pairwise comparison of traveling/lingering scores using one-way ANOVA with Bonferroni correction.

5.5 Transition dynamics

Depression heterogeneity was also evident when comparing the transition dynamics in some networks. As shown in Figure 5.5-b, there were significant differences between non-melancholic and melancholic groups in traveling scores ($p < 0.05$; *N vs. M*; *DDMN*), and lingering scores ($p < 0.01$; *N vs. M*; *DDMN*, *LECN*) of individual participants. There were also significant group differences in the lin-

gering scores between healthy and non-melancholic($p < 0.01$; *H vs. N*; *DDMN*) and healthy and melancholic groups ($p < 0.01$; *H vs. M*; *DDMN*, *LECN*). Furthermore, there is significant increase in lingering scores of melancholic group in LECN ($Lingering = 0.61 \pm 0.06$) as compared to non-melancholic ($Lingering = 0.55 \pm 0.06$; $p < 0.005$) and healthy groups ($Lingering = 0.53 \pm 0.06$; $p < 0.005$). Results for other functional networks are listed in Table D.3.

5.6 Minor changes between model frameworks

The materials and methods discussed in Section 2 mainly applied to our singular and separate models for the healthy and the depressed groups, as discussed further in *Chapter 3 - Singular Model for Depression Biomarker* and *Chapter 4 - Separate Model for Major Depression*. However, as we explored the new model discussed in this section, the following minor changes were made:

- In terms of data, we split the depressed group into melancholic and non-melancholic subgroups based on the melancholic criteria in the MINI interview [51].
- Instead of a singular P-MEM, we generated a P-MEM for the healthy, non-melancholic, and melancholic groups, similar to the separate model framework (Figure 4.1).
- Consequently, group-level features such as basin energy and basin size were compared across groups.
- While individual-level features such as basin occurrence and transition dynamics scores were computed on the parameters of the P-MEM corresponding to the participants' group.
- One-One-way Analysis of Variance (ANOVA) was performed to find significant group differences (healthy vs. non-melancholic vs. melancholic) in participants' age, IQ, BDI-II, and SHAPS (Snaith-Hamilton Pleasure Scale) scores. Bonferroni correction was applied to compensate for multiple group comparisons.

- Finally, we also investigated the correlation between depressive symptoms (BDI-II, SHAPS) and basin characteristics (basin occurrence frequency). Multivariate linear regression models were fitted on the data, with $p < 0.05$ deemed a statistically significant relationship between the variables.

6 Discussions and Limitations

DSM-V classifies melancholic depression under "major depressive disorder with melancholic features". While we used the term *subtype* throughout this dissertation, according to DSM-V, melancholia is technically called a *specifier* for depression [10]. Whereas a subtype is unique and exclusive (there are currently no subtypes for MDD), a specifier is more inclusive and may coexist with other specifiers. However, this dissertation's consistent use of the term *subtype* when referring to melancholic depression was intentional. Treating melancholic depression this way homogenizes a subgroup of MDD—as opposed to melancholia merely being one of the "add-on" flavors, so to speak—, and it respects several accounts of melancholic depression as distinct to non-melancholic, atypical, and other subtypes of MDD [25, 73, 74, 78].

6.1 Depression heterogeneity

Depression heterogeneity has plagued research advancement on the diagnosis and treatment of the disorder [14, 79, 80]. Considerable efforts have been made towards drawing boundaries within the currently accepted definition of major depressive disorder [79, 80], suggesting that investigations on depressive symptoms and their interactions may lead to discoveries [14]. In this study, one of our goals was to show heterogeneity in the depressed participants. Our analysis results have confirmed the heterogeneous aspects of the depression data, as observed from significant differences between melancholic and non-melancholic groups in BDI-II and anhedonia scores (Table 2.1); basin frequencies across 12 networks (Table D.1); and transition dynamics scores in DDMN, LECN, PSN, RECN, VDMN, and VSPN (Table D.3).

6.2 Melancholia and depression severity

Melancholic depression is associated with greater symptom severity than depression with non-melancholic features [73–75]. This association was evident in our individual-level analysis of BDI-II scores, where the melancholic group scored significantly higher than the other groups (Table 2.1).

Readers may wonder if energy landscape features can be a proxy for evaluating some symptoms associated with melancholic features. We performed regression analysis on basin frequencies and depression severity score (BDI-II) to check this possibility. However, despite having clear boundaries among the groups, no significant correlation was found in any network (e.g., DDMN in Figure 6.1-a).

The order of increasing severity from healthy, to non-melancholic, to melancholic depression, may seem intuitive. However, some studies argue against the severity-based categorization of melancholic depression [81, 82] and do not identify melancholia as a "more severe" form of depression [82]. This pattern is evident in Figure 6.1-a, where the BDI-II scores for non-melancholic and melancholic groups coincide. We can further argue that the basin frequency of our energy landscape model was more effective than the depressive scores (BDI-II and SHAPS) in discriminating melancholic depression.

6.3 Melancholia and anhedonia

Following depression severity, we then tested if the correlation with basin frequency would also hold for anhedonia. Anhedonia is one of the overlapping symptoms of melancholia and depression [70, 73]. This effect was apparent in the participants' demographic data, where the melancholic group had a significantly higher SHAPS score (Table 2.1).

Similar to BDI-II scores, there was no significant correlation between SHAPS scores and basin frequencies (Figure 6.1-b). However, a closer inspection of results

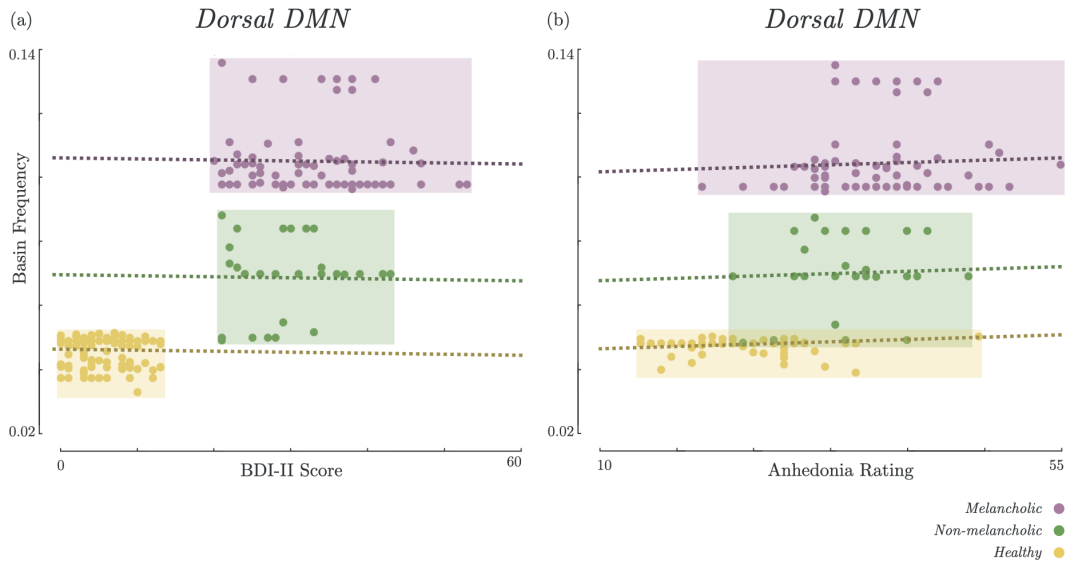

Figure 6.1: Correlation of basin frequencies to depressive symptoms

Correlation between average basin frequency and depressive symptom (a. depression severity; b. anhedonia) on DDMN.

Dotted lines correspond to multivariate linear regression model $y = \alpha_1 z_1 + \alpha_2 z_2 + \beta x$; y: basin frequency, x: symptom score; z_1: dummy variable for non-melancholic; z_2: dummy variable for melancholic; α, β: regression coefficients. No significant correlations between basin frequency and depression symptom (regression t-test $p_{BDI} = 0.7910$, $p_{Anhedonia} = 0.3339$).

Boxes delineate the range of data points for each group (yellow: healthy; green: non-melancholic; purple: melancholic).

in the DDMN revealed an apparent connection between these features. Studies report that the decrease in functional connectivity of dorsomedial prefrontal cortex ($dmPFC$) with posterior cingulate cortex/precuneus ($PCC/PCUN$) is related to depression severity and anhedonia [35, 83]. Looking at the major basins found by our model in DDMN (Figure 5.2), the major basin pairs for all groups had anti-synchronized activations of mPFC and PCUN ($S_{279} : \{mPFC = 1, PCC/PCUN = 0\}$, H, N, M; $S_{232} : \{mPFC = 0, PCC/PCUN = 1\}$, H, M; $S_{168} : \{mPFC = 1, PCC/PCUN = 0\}$, N). This decoupling between mPFC and PCC/PCUN may be attributed to impaired reward anticipation, a key anhedonia feature [83]. Although current research has not established the direct

connection between dynamic functional connectivity and the energy landscape model [43], our results may provide insight into the potential connection between these models.

6.4 Melancholia and rumination

Lastly, we investigated the possible presence of ruminative states in the energy landscapes. Rumination tends to dwell on the same—usually negative—thoughts for prolonged periods. Since studies have shown a significant correlation of rumination to both melancholia [84] and depression [85], we explored the energy landscape characteristics to provide more evidence on this correlation. Ruminative thinking is marked by increased connectivity in DMN [86] and decreased activity in the left dorsolateral prefrontal cortex (*left dlPFC*; equivalent to *LECN*) [87]. In terms of our energy landscape model, we defined dynamic activity as transitioning from one basin to another. This activity was in contrast to static activity, which stays at the same basin. We derived two measures for brain activity: *traveling score* (Equation 2.16) for dynamic activity, and *lingering score* (Equation 2.17) for static activity. Thus, a high traveling score and a low lingering score would imply a more active network.

The significant increase of lingering scores of the melancholic group in LECN (Figure 5.5) may imply that the melancholic group had a greater tendency to be "stuck" in a basin or within its cluster. This pattern may also be related to the decreased activity in the left dlPFC found in rumination [87]. On the contrary, in the dorsal part of DMN (DDMN), the lingering scores of melancholic group ($Lingering = 0.55 \pm 0.07$) were significantly lower than healthy ($Lingering = 0.58 \pm 0.06$; $p < 0.01$) and non-melancholic groups ($Lingering = 0.63 \pm 0.05$; $p < 0.005$). Although this may support previous studies showing increased connectivity in DMN during ruminative thinking, analyzing the lingering scores in the ventral part of DMN (*VDMN*) led to contradicting results [86]. Nevertheless, the traveling scores in DDMN were significantly higher in melancholic group ($Traveling = 0.10 \pm 0.09$) than in non-melancholic group

($Traveling = 0.05 \pm 0.06$; $p < 0.05$). For LECN and VDMN, there were no significant differences in traveling scores between groups.

6.5 Limitations

Unlike typical functional connectivity (FC) models that are based on the correlation between two regions (i.e., using Pearson's correlation coefficient), the ELA model does not assume that pairwise interactions of regions are independent of each other [37]. This freedom from assumption allowed our model to more accurately capture the global activity patterns that may be overlooked by FC-based models [37]. Some FC-based studies tried to work around this limitation by using a different FC metric (such as precision matrix) or by introducing a sliding window in the analysis (also known as dynamic FCA) [88].

Hidden Markov Model (HMM) is another standard brain dynamics model for resting-state fMRI. Compared to ELA, which utilizes pairwise MEM, HMM is more complex and maybe more expressive [89]. Thus, our ELA results may serve as a baseline for future analysis on brain dynamics of melancholic depression using models such as HMM.

Furthermore, our present study has other limitations. ELA assumes a memoryless process, such that predicting the next state only depends on the current state and not the past states [43]. This memorylessness saves us memory space and processing time [90], but this only works on systems at equilibrium, which typically requires a considerable amount of data [44]. We decided to use resting-state fMRI data to address this problem since these are expected as equilibrium states [91]. Then, we combined the fMRI time signals of all group participants to produce "long" temporal data. Since there are substantially more healthy participants, the model for the healthy group may have converged closer to equilibrium than the two depressed subgroups.

Although concatenation of individual fMRI data should only have minimal effect on our analysis due to the "memorylessness" aspect of ELA [45], it should

be noted that combining participants' fMRI data could still potentially introduce bias due to BOLD signal differences across participants. We addressed this by using individual participants' mean fMRI BOLD signals as the threshold for binarizing the signals. However, it is recommended to investigate further the implications of data concatenation and mitigate the intensity differences in individual fMRI.

We must also reconsider the effects of each data preprocessing technique on the analysis outcome. For example, global signal regression may significantly impact resting-state connectivity results, especially when comparing groups with different signal characteristics [43, 92]. The frequency band for band-pass filtering may exclude important information such as the amplitude of low-frequency fluctuations (ALFF) during rumination [93]. The filtering of middle-ground individuals (i.e., healthy participants with relatively high BDI scores and depressed participants with low BDI scores) certainly affects analysis results related to depression severity. Even the binarization of signals should be reexamined in the context of depressive symptoms, despite being shown to preserve signal LFP and topological brain data [45].

Our selection of ROIs relies on the parcellation method (Shirer Atlas [59]) and data availability. As such, we removed some ROIs due to unreliable or insufficient data. The inclusion of these ROIs might affect the results. Choosing a different parcellation method might also produce different results. It is also possible to study a more extensive scale of networks that are not constrained to the functional mapping of the ROIs used in this study [44, 46, 61, 65]. Thus, testing the robustness and consistency of our model on different sets of ROIs or with different parcellation methods would be a reasonable step moving forward.

It is often pointed out that the site difference could be a potential confounding factor for the observed BOLD signals [94]. When we applied two-way ANOVA considering two factors of participant groups and site ID to basin frequencies, all main effects, and their interaction were statistically significant (Table D.1). While this still supports that basin frequencies across different networks could differentiate participants suffering from melancholic and non-melancholic MDD

at a population level, its reliability as a biomarker for personalized medicine should never be overestimated. Thus, the potential site bias is a limitation in the present study, and we should address the issue in our future work.

Even though we hypothesized *a priori* that the energy landscape of melancholic depression will be different from non-melancholic due to depression heterogeneity, our analyses and interpretations of the results were made *post-hoc*. For statistical analyses, we applied Bonferroni correction to compensate for multiple comparison tests that would increase the risk of Type 1 error [95].

Our discussion on the relation between melancholia and rumination is more suggestive than conclusive since we lack rumination quantifiers to analyze with our models. In the future, it would be crucial to record the ruminative tendencies of participants using standardized measures such as the Ruminative Response Scale (RRS) [96].

It is important to remember that melancholia, in itself, is also heterogeneous [97]. Multiple symptoms characterize it, and thus its severity and symptoms may vary from one person to another. Current biomarker models focus on the distinguishing features of melancholic depression on a group level [98–100]. Although ELA allows us to study the group-wide brain dynamics of melancholic depression and the individual nuances in brain states and functional region interactions, focusing more on these individual differences would allow us to confront heterogeneity directly.

6.6 Recommendations for future work

Finally, the results discussed in this study opened several theoretical and practical avenues that would require more time and effort to inspect further. We want to close this discussion with our recommended research directions for future extensions of this study.

6.6.1 Energy landscape analysis and statistical tools

In this study, we have taken a by-the-book approach concerning our methodology for energy landscape analysis. In order to achieve more novel results, these are the questions that might be of interest: *What would happen if we do not distinguish between major and minor basins? How about if we analyze one basin at a time? What other metrics can we use to measure brain dynamics from the model? How can we test for noise and other effects in the energy landscape features?* Moreover, there are more modern tools for inferring statistical differences than the tools used in this study. Applying these tools would help validate our results and uncover new ones.

6.6.2 Psychophysiological interpretation of the model

Interpretability is one of our main reasons for choosing the energy landscape model. However, ELA has not been applied to depression studies by other researchers during this writing. Thus, our interpretations of the possible psychophysiological mechanisms behind the analysis results must be cross-checked. These interpretations include the basins: *What are the neurological basis for basins? How are anti-synchronous basins related to cognitive functions?*; traveling/efficiency scores: *Does a healthy brain always have an efficient network? Is there a traveling score threshold for depression*; lingering scores: *How do lingering scores reflect network activity in the context of rumination? Would other concentrated cognitive tasks such as focused thinking reflect high lingering scores as well?*. Aside from probing these questions, it may also be helpful to conduct replicability studies (if possible, on the same individuals) to check if the model is robust to resting-state data.

6.6.3 Correlation of model and clinical features

Lastly, the end goal of this study is to improve the clinical diagnosis of depression. We need to find the relationship between the model features and clinical features for depression to achieve this goal. On the modeling aspect, we recommend applying more powerful tools such as multivariate analysis and machine learning methods in building the correlation/classifier model. On the clinical side, adding more features such as ruminative scores (RRS) can account for the other inherent variances in the heterogeneous major depressive disorder. In our current dataset, some patients had comorbid symptoms such as suicidality, alcohol abuse, and anxiety disorder (see Table A.1). Thus, it is also essential to look into the history of depressed individuals to develop a more comprehensive energy landscape model for depression, which covers various comorbidities, treatment responses, and recurrences.

7 Conclusion

There were two goals in this study. Initially, we wanted to discover biomarkers for MDD based on neurodynamic features from the energy landscape model. Later on, we wanted to characterize the distinguishing neurodynamic features of melancholic depression. Both of these goals were connected to the core problem of depression heterogeneity.

7.1 Research contributions

With our separate model framework for melancholic depression, we found distinguishing energy landscape features of melancholic depression, which included major basin energy barriers, basin frequency, and state transition dynamics. Statistical results were consistent across our analyses on 12 functional brain networks, indicating our model's robustness. Moreover, these results agree with existing studies on melancholic features, such as depression severity [35, 74, 75], anhedonia [35, 83], and rumination [84, 87]. These results, when taken together, provide strong evidence that melancholic depression is a distinct disorder with recognizable neurodynamic patterns that explain mental processes.

7.2 Finding biomarkers for depression

Finally, we have not given up on our pursuit of biomarkers for depression. Our initial attempts gave us first-hand experience of the challenges researchers face when studying MDD. Moving forward, we recommend that researchers shift their focus to depression subtypes, as our current notion of major depressive disorder

may be counterproductive to giving the proper treatment to patients. After all, the entirety of this study will be for naught if depressed people will not be provided with the opportunity to live normal lives.

Acknowledgments

This dissertation has been a product of countless hours of research, which would not have been successful without the support and guidance I have received from the following people and organizations.

To my supervisors, Prof. Ikeda and Prof. Yoshimoto, who went above and beyond when guiding me throughout my doctoral course: thank you.

To my lab colleagues, my tutor Eri, my seat buddy Igor, and the rest of Mathematical Informatics Lab, who gave me valuable feedback during seminars: thank you.

To my other mentors, my Japanese language teacher Yoko-sensei, my martial arts teacher Hayashi-shifu, and Templish director Hide-san, who helped me become a well-rounded person: thank you.

To NAIST, UPD, and ERDT, our lab secretaries Miss Aya and Miss Yasuki, our department administrators Maam Grace and Maam Judith, and my scholarship coordinator Maam Kath, who patiently and cordially assisted me with my academic and non-academic concerns: thank you.

To Sir JM, who opened the door for me to study at NAIST: thank you.

To my friends in NAIST, Dianne, Chi, Peki, Julian, Xian, Nicko, Romeo, Mark, Josh, Abi, Tsuyoshi, Aimi, Lily, my board game buddies, photography pals, and everyone who made me a better version of myself: thank you.

To my colleagues in DCS, my friends in the Philippines, and my former students who kept me grounded and excited for the future: thank you.

To my family, my mom, my dad, my kuya and our bunso, who always supported me behind the scenes and longed for my return: thank you.

And to my God, my light and redeemer, who helped me walk whenever my feet would fail: thank you.

Appendices

A Data Set and ROI

Table A.1: Demographic data and MINI symptoms of subjects

		Depressed		
	Healthy	Non-Melancholic	Melancholic	P-value
No. of participants	142	31	89	
Sex (female / male)[1]	71 / 71	16 / 15	44 / 45	
Age (years)[2]	42.62 ± 14.33	41.48 ± 9.46	43.37 ± 11.65	
BDI-II[2]	5.34 ± 3.76	29.13 ± 6.08	32.40 ± 7.88	(∗)(∗∗∗)
Anhedonia (SHAPS)[2]	23.27 ± 6.20	34.21 ± 5.30	37.72 ± 6.22	(∗)(∗∗∗)
IQ (JART)[2]	110.92 ± 8.813	114.09 ± 9.57	111.61 ± 9.30	
Site participants (HUH/HRC/HKH/COI)[1]	44 / 32 / 20 / 46	10 / 6 / 7 / 8	48 / 7 / 13 / 21	(∗∗)
Time samples per participant	161.90 ± 45.51	156.68 ± 50.34	155.39 ± 40.89	
MINI symptoms				
Major depressive disorder	0	89	31	
Dysthymic disorder	0	0	0	
Suicidality	9	47	21	
Mania	3	9	1	
Panic disorder	0	3	2	
Agoraphobia	2	10	2	
Social phobia	0	17	5	
Obsessive-compulsive disorder	0	3	0	
Post-traumatic stress disorder	0	0	0	
Alcohol abuse	0	8	3	
Drug dependence / abuse	0	0	0	
Psychotic disorder	0	2	0	
Anorexia nervosa	0	3	0	
Bulimia	0	1	0	
Generalized anxiety disorder	0	4	0	
Antisocial personality disorder	0	0	0	

BDI-II, Beck Depression Inventory-II; SHAPS, Snaith-Hamilton Pleasure Scale; JART, Japanese Adult Reading Test
Recruitment sites: Hiroshima University Hospital (HUH), Hiroshima Rehabilitation Center (HRC), Hiroshima Kajikawa Hospital (HKH), Center of Innovation in Hiroshima University (COI)

[1] Multiple group comparison using pairwise Chi-squared tests
[2] Multiple group comparison using one-way ANOVA with Bonferroni correction

(∗) $p < 0.05$ between non-melancholic and melancholic groups
(∗∗) $p < 0.01$ between healthy and melancholic groups
(∗∗∗) $p < 0.005$ between healthy and non-melancholic groups, and between healthy and melancholic groups

The functional networks analyzed in this study are summarized in Table A.2. Here, the anatomical regions are listed for each ROI. Note that the ordering is important for defining the brain states, such that given ROIs $[\,R_1\ R_2\ R_3\,]$, the state S_1 corresponds to activated regions $[\,0\ 0\ 1\,]$. In other words, the state index is equivalent to the binary representation of the activated regions in the state ($index_{10} = activation_2$).

Table A.2: Complete list of functional brain networks and ROIs

Network		Anatomical Locations of Functional ROIs
Auditory Network (AN)	(1)	Left Superior Temporal Gyrus, Heschl's Gyrus
	(2)	Right Superior Temporal Gyrus
	(3)	Right Thalamus
Anterior Salience Network (ASN)	(1)	Left Middle Frontal Gyrus
	(2)	Left Insula
	(3)	Anterior Cingulate Cortex, Medial Prefrontal Cortex, Supplementary Motor Area
	(4)	Right Middle Frontal Gyrus
	(5)	Right Insula
Basal Ganglia Network (BGN)	(1)	Left Thalamus, Caudate
	(2)	Right Thalamus, Putamen
	(3)	Left Inferior Frontal Gyrus
	(4)	Right Inferior Frontal Gyrus
	(5)	Pons
Dorsal Default Mode Network (DDMN)	(1)	Medial Prefrontal Cortex, Anterior Cingulate Cortex, Orbitofrontal Cortex
	(2)	Left Angular Gyrus
	(3)	Right Superior Frontal Gyrus
	(4)	Posterior Cingulate Cortex, Precuneus
	(5)	Midcingulate Cortex
	(6)	Right Angular Gyrus
	(7)	Left and Right Thalamus
	(8)	Left Hippocampus
	(9)	Right Hippocampus
Language Network (LN)	(1)	Inferior Frontal Gyrus
	(2)	Left Middle Temporal Gyrus
	(3)	Left Middle Temporal Gyrus, Angular Gyrus
	(4)	Left Middle Temporal Gyrus, Superior Temporal Gyrus, Supramarginal Gyrus, Angular Gyrus
	(5)	Right Inferior Frontal Gyrus
	(6)	Right Supramarginal Gyrus, Superior Temporal Gyrus, Middle Temporal Gyrus

Table A.2: Complete list of functional brain networks and ROIs (continued)

Network		Anatomical Locations of Functional ROIs
Left Executive Control Network (LECN / L-DLPFC)	(1)	Left Middle Frontal Gyrus, Superior Frontal Gyrus
	(2)	Left Inferior Frontal Gyrus, Orbitofrontal Gyrus
	(3)	Left Superior Parietal Gyrus, Inferior Parietal Gyrus, Precuneus, Angular Gyrus
	(4)	Left Inferior Temporal Gyrus, Middle Temporal Gyrus
	(5)	Left Thalamus
Precuneus Network (PN)	(1)	Midcingulate Cortex, Posterior Cingulate Cortex
	(2)	Precuneus
	(3)	Left Angular Gyrus
	(4)	Right Angular Gyrus
Posterior Salience Network (PSN)	(1)	Left Middle Frontal Gyrus
	(2)	Left Supramarginal Gyrus, Inferior Parietal Gyrus
	(3)	Left Precuneus
	(4)	Right Midcingulate Cortex
	(5)	Right Superior Parietal Gyrus, Precuneus
	(6)	Right Supramarginal Gyrus, Inferior Parietal Gyrus
	(7)	Left Thalamus
	(8)	Left Posterior Insula, Putamen
	(9)	Right Thalamus
	(10)	Right Posterior Insula
Right Executive Control Network (RECN / R-DLPFC)	(1)	Right Middle Frontal Gyrus, Right Superior Frontal Gyrus
	(2)	Right Middle Frontal Gyrus
	(3)	Right Inferior Parietal Gyrus, Supramarginal Gyrus, Angular Gyrus
	(4)	Right Superior Frontal Gyrus
	(5)	Right Caudate
Sensorimotor Network (SMN)	(1)	Left Precentral Gyrus, Postcentral Gyrus
	(2)	Right Precentral Gyrus, Postcentral Gyrus
	(3)	Right Supplementary Motor Area
	(4)	Left Thalamus
	(5)	Right Thalamus
Ventral Default Mode Network (VDMN)	(1)	Left Retrosplenial Cortex, Posterior Cingulate Cortex
	(2)	Left Middle Frontal Gyrus
	(3)	Left Parahippocampal Gyrus
	(4)	Left Middle Occipital Gyrus
	(5)	Right Retrosplenial Cortex, Posterior Cingulate Cortex
	(6)	Precuneus
	(7)	Right Superior Frontal Gyrus, Middle Frontal Gyrus
	(8)	Right Parahippocampal Gyrus
	(9)	Right Angular Gyrus, Middle Occipital Gyrus
Visuospatial Network (VSPN)	(1)	Left Middle Frontal Gyrus, Superior Frontal Gyrus, Precentral Gyrus
	(2)	Left Inferior Parietal Sulcus
	(3)	Left Frontal Operculum, Inferior Frontal Gyrus
	(4)	Left Inferior Temporal Gyrus
	(5)	Right Middle Frontal Gyrus
	(6)	Right Inferior Parietal Lobule
	(7)	Right Frontal Operculum, Inferior Frontal Gyrus
	(8)	Right Middle Temporal Gyrus

B Singular Model Results

Complete results of energy landscape analyses for the singular model framework (Section 3) are presented here. Analyses were conducted on the combined data of healthy and depressed groups, and on each functional network (Table A.2).

Table B.1: Singular model: Basin occurrence frequency

Network	Healthy	Depressed	Network	Healthy	Depressed
AN	0.6352 ± 0.03	0.6409 ± 0.03	PN	0.6878 ± 0.01	0.6893 ± 0.01
ASN	0.2819 ± 0.01	0.2798 ± 0.01	PSN	0.0752 ± 0.01	0.0757 ± 0.01
BGN	0.5925 ± 0.02	0.5958 ± 0.02	RECN	0.4114 ± 0.01	0.4109 ± 0.01
DDMN	0.0476 ± 0.00	0.0476 ± 0.01	SMN	0.4381 ± 0.04	0.4448 ± 0.03
LN	0.2279 ± 0.01	0.2257 ± 0.01	VDMN	0.0994 ± 0.01	0.0982 ± 0.01
LECN	0.2373 ± 0.02	0.2395 ± 0.02	VSPN	0.1339 ± 0.01	0.1349 ± 0.01

Table B.2: Singular model: Basin characteristics

Network	B	E	Size
AN	1	-3.01	50.00 %
	6	-2.98	50.00 %
ASN	9	-1.84	43.75 %
	22	-1.82	43.75 %
	3	-0.87	6.25 %
	28	-0.85	6.25 %
BGN	6	-1.96	25.00 %
	25	-1.96	25.00 %
	26	-1.52	15.62 %
	5	-1.49	15.62 %
	28	-1.45	9.38 %
	3	-1.43	9.38 %
DDMN	279	-3.31	45.31 %
	232	-3.27	44.92 %
	340	-1.69	4.30 %
	171	-1.64	4.30 %
	419	-1.26	0.59 %
	92	-1.23	0.59 %
LN	34	-1.51	37.50 %
	29	-1.51	37.50 %
	56	-1.17	10.94 %
	7	-1.16	10.94 %
	19	-0.92	1.56 %
	44	-0.90	1.56 %
LECN	28	-1.06	46.88 %
	3	-1.05	46.88 %
	5	-0.67	3.12 %
	26	-0.65	3.12 %
PN	12	-1.46	37.50 %
	3	-1.43	37.50 %
	10	-0.85	6.25 %
	5	-0.79	6.25 %
	9	-0.61	6.25 %
	6	-0.59	6.25 %
PSN	789	-2.89	14.45 %
	234	-2.88	14.36 %
	527	-2.83	15.62 %
	496	-2.77	15.92 %
	79	-2.65	7.42 %
	794	-2.57	9.96 %
	229	-2.56	9.67 %
	944	-2.56	7.42 %
	287	-2.21	2.15 %
	736	-2.18	2.34 %
	117	-1.78	0.68 %
RECN	28	-1.08	40.62 %
	3	-1.07	34.38 %
	10	-0.96	6.25 %
	9	-0.95	6.25 %
	22	-0.93	6.25 %
	21	-0.93	6.25 %
SMN	3	-2.06	50.00 %
	28	-2.02	50.00 %
VDMN	165	-2.81	21.48 %
	346	-2.80	21.88 %
	206	-2.79	23.05 %
	305	-2.75	20.90 %
	99	-1.81	5.66 %
	404	-1.78	7.03 %
VSPN	85	-2.80	22.27 %
	170	-2.76	21.09 %
	51	-2.16	21.09 %
	204	-2.16	19.92 %
	102	-1.77	6.25 %
	153	-1.75	6.25 %
	240	-1.19	1.56 %
	15	-1.16	1.56 %

Basin states, their energy and cluster size. See Section A for details on state indexing.

Major basins are listed on first two rows (highlighted in purple) for each group and network. Unique basins are shaded in light purple. For each group, basins are sorted from lowest energy, and then from largest size.

Table B.3: Singular model: Major basins transition dynamics

Network	Score	Healthy	Depressed	Network	Score	Healthy	Depressed
AN	Traveling	0.91 ± 0.37	0.89 ± 0.31	PN	Traveling	0.83 ± 0.31	0.82 ± 0.27
	Lingering	0.48 ± 0.06	0.48 ± 0.06		Lingering	0.29 ± 0.07	0.29 ± 0.06
	TR(A)	0.15 ± 0.04	0.15 ± 0.03		TR(A)	0.10 ± 0.03	0.10 ± 0.03
	TR(P)	0.18 ± 0.04	0.18 ± 0.04		TR(P)	0.12 ± 0.03	0.12 ± 0.03
	SR(A)	0.31 ± 0.09	0.31 ± 0.08		SR(A)	0.18 ± 0.07	0.18 ± 0.07
	SR(P)	0.17 ± 0.07	0.17 ± 0.07		SR(P)	0.11 ± 0.04	0.11 ± 0.03
ASN	Traveling	0.38 ± 0.23	0.37 ± 0.18	PSN	Traveling	0.05 ± 0.08	0.05 ± 0.07
	Lingering	0.40 ± 0.07	0.40 ± 0.07		Lingering	0.10 ± 0.05	0.10 ± 0.04
	TR(A)	0.08 ± 0.04	0.08 ± 0.03		TR(A)	0.00 ± 0.01	0.00 ± 0.01
	TR(P)	0.21 ± 0.04	0.21 ± 0.04		TR(P)	0.09 ± 0.02	0.09 ± 0.02
	SR(A)	0.09 ± 0.06	0.09 ± 0.06		SR(A)	0.00 ± 0.01	0.00 ± 0.01
	SR(P)	0.32 ± 0.10	0.31 ± 0.08		SR(P)	0.10 ± 0.05	0.10 ± 0.04
BGN	Traveling	0.78 ± 0.42	0.76 ± 0.33	RECN	Traveling	0.28 ± 0.14	0.27 ± 0.13
	Lingering	0.19 ± 0.08	0.18 ± 0.07		Lingering	0.28 ± 0.07	0.28 ± 0.06
	TR(A)	0.08 ± 0.03	0.07 ± 0.03		TR(A)	0.04 ± 0.02	0.04 ± 0.02
	TR(P)	0.11 ± 0.03	0.10 ± 0.03		TR(P)	0.16 ± 0.04	0.16 ± 0.04
	SR(A)	0.11 ± 0.07	0.10 ± 0.05		SR(A)	0.04 ± 0.03	0.04 ± 0.02
	SR(P)	0.08 ± 0.03	0.08 ± 0.03		SR(P)	0.25 ± 0.06	0.24 ± 0.06
DDMN	Traveling	0.09 ± 0.08	0.08 ± 0.08	SMN	Traveling	0.37 ± 0.15	0.37 ± 0.15
	Lingering	0.56 ± 0.06	0.57 ± 0.06		Lingering	0.50 ± 0.06	0.49 ± 0.06
	TR(A)	0.02 ± 0.02	0.02 ± 0.02		TR(A)	0.09 ± 0.03	0.09 ± 0.03
	TR(P)	0.23 ± 0.04	0.23 ± 0.04		TR(P)	0.25 ± 0.04	0.25 ± 0.05
	SR(A)	0.02 ± 0.02	0.01 ± 0.02		SR(A)	0.13 ± 0.07	0.13 ± 0.07
	SR(P)	0.55 ± 0.07	0.55 ± 0.06		SR(P)	0.36 ± 0.09	0.36 ± 0.09
LN	Traveling	0.17 ± 0.11	0.17 ± 0.09	VDMN	Traveling	0.08 ± 0.11	0.07 ± 0.10
	Lingering	0.38 ± 0.07	0.38 ± 0.06		Lingering	0.22 ± 0.06	0.21 ± 0.06
	TR(A)	0.03 ± 0.02	0.03 ± 0.02		TR(A)	0.01 ± 0.01	0.01 ± 0.01
	TR(P)	0.20 ± 0.04	0.20 ± 0.04		TR(P)	0.13 ± 0.03	0.13 ± 0.03
	SR(A)	0.03 ± 0.02	0.03 ± 0.02		SR(A)	0.01 ± 0.01	0.01 ± 0.01
	SR(P)	0.35 ± 0.07	0.35 ± 0.06		SR(P)	0.21 ± 0.06	0.21 ± 0.06
LECN	Traveling	0.17 ± 0.09	0.17 ± 0.09	VSPN	Traveling	0.19 ± 0.13	0.18 ± 0.14
	Lingering	0.53 ± 0.06	0.53 ± 0.06		Lingering	0.17 ± 0.07	0.17 ± 0.06
	TR(A)	0.04 ± 0.02	0.04 ± 0.02		TR(A)	0.02 ± 0.02	0.02 ± 0.02
	TR(P)	0.24 ± 0.03	0.24 ± 0.03		TR(P)	0.12 ± 0.03	0.12 ± 0.03
	SR(A)	0.04 ± 0.03	0.04 ± 0.03		SR(A)	0.02 ± 0.03	0.02 ± 0.03
	SR(P)	0.49 ± 0.07	0.49 ± 0.07		SR(P)	0.15 ± 0.06	0.15 ± 0.05

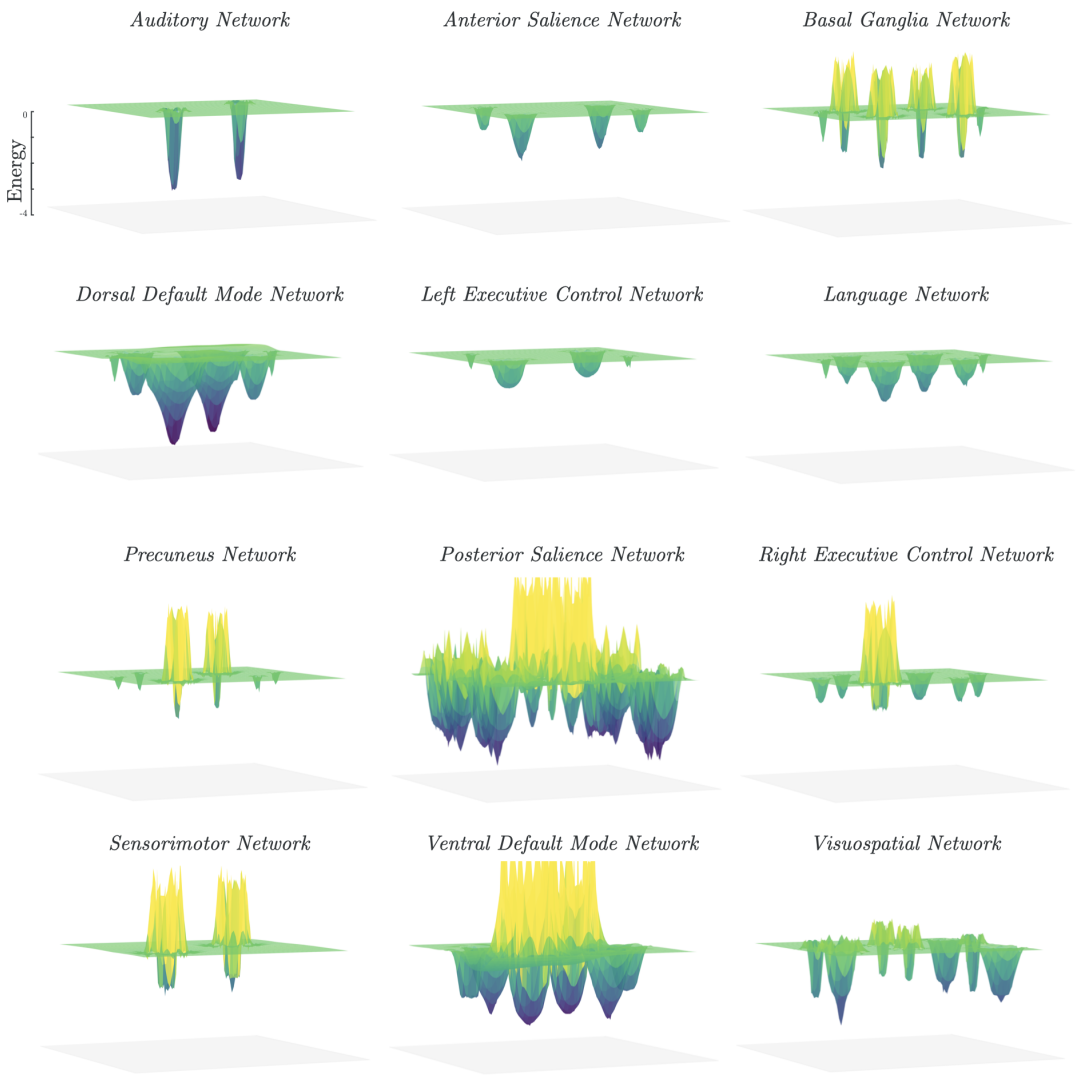

Figure B.1: Singular model: Energy landscapes

3D representations of energy landscapes across groups and networks. Basins and clusters are plotted on arbitrary state space; i.e. x- and y-locations are arbitrary. Basin sizes are proportional to the number of neighboring states clustered (Section 2.5). See Supplementary Table B.2 for detailed information on individual basins.

C Separate Model Results

Complete results of energy landscape analyses for the separate model framework (Section 4) are presented here. Analyses were conducted separately for healthy and depressed groups, and on each functional network (Table A.2).

Table C.1: Separate model: Basin occurrence frequency

	Basin frequency		p-value	
Network	Healthy	Depressed	ANOVA	KW
AN	0.6352 ± 0.03	0.5976 ± 0.03	***	***
ASN	0.2819 ± 0.01	0.3910 ± 0.04	***	***
BGN	0.5925 ± 0.02	0.6335 ± 0.01	***	***
DDMN	0.0462 ± 0.00	0.1333 ± 0.01	***	***
LN	0.2279 ± 0.01	0.1995 ± 0.01	***	***
LECN	0.2373 ± 0.02	0.1869 ± 0.03	***	***
PN	0.6878 ± 0.01	0.6500 ± 0.03	***	***
PSN	0.0870 ± 0.01	0.0925 ± 0.01	***	
RECN	0.4114 ± 0.01	0.3208 ± 0.03	***	***
SMN	0.4381 ± 0.04	0.3046 ± 0.02	***	***
VDMN	0.0601 ± 0.02	0.0850 ± 0.01	***	***
VSPN	0.1339 ± 0.01	0.2049 ± 0.00	***	***

Occurrence frequency (mean ± std) of basins on individual participants' fMRI time signals.

(***) $p < 0.005$; between-group comparison of basin frequencies using one-way ANOVA and Kruskal-Wallis test

Table C.2: Separate model: Basin characteristics

Network	Healthy B	Healthy E	Healthy Size	Depressed B	Depressed E	Depressed Size
AN	1	-3.00	50.00 %	1	-3.02	50.00 %
	6	-2.97	50.00 %	6	-2.99	50.00 %
ASN	9	-1.78	43.75 %	9	-1.91	43.75 %
	22	-1.74	43.75 %	22	-1.90	43.75 %
	3	-0.85	6.25 %	3	-0.90	6.25 %
	28	-0.83	6.25 %	28	-0.87	6.25 %
BGN	6	-1.92	25.00 %	6	-2.01	28.12 %
	25	-1.92	25.00 %	25	-2.01	28.12 %
	26	-1.51	15.62 %	26	-1.54	12.50 %
	28	-1.48	9.38 %	5	-1.52	12.50 %
	3	-1.47	15.62 %	28	-1.41	9.38 %
	5	-1.47	9.38 %	3	-1.38	9.38 %
DDMN	279	-3.32	45.70 %	279	-3.30	44.53 %
	232	-3.29	46.29 %	232	-3.25	44.14 %
	340	-1.68	3.71 %	340	-1.71	4.69 %
	171	-1.63	3.71 %	171	-1.67	5.08 %
	419	-1.29	0.59 %	419	-1.24	0.59 %
				92	-1.18	0.59 %
				404	-1.14	0.39 %
LN	29	-1.51	37.50 %	34	-1.51	43.75 %
	34	-1.51	37.50 %	29	-1.50	43.75 %
	56	-1.19	10.94 %	56	-1.15	6.25 %
	7	-1.19	10.94 %	7	-1.13	6.25 %
	19	-0.95	1.56 %			
	44	-0.93	1.56 %			
LECN	28	-1.03	46.88 %	28	-1.11	50.00 %
	3	-1.03	46.88 %	3	-1.09	50.00 %
	5	-0.68	3.12 %			
	26	-0.68	3.12 %			

Basin states, their energy and cluster size. See Section A for details on state indexing.
Major basins are listed on first two rows (highlighted in purple) for each group and network. Unique basins are shaded in light purple. For each group, basins are sorted from lowest energy, and then from largest size.

Table C.2: Separate model: Basin characteristics (continued)

	Healthy			Depressed		
Network	B	E	Size	B	E	Size
PN	12	-1.49	37.50 %	12	-1.43	37.50 %
	3	-1.43	37.50 %	3	-1.41	37.50 %
	10	-0.87	6.25 %	10	-0.82	6.25 %
	5	-0.81	6.25 %	5	-0.77	6.25 %
	6	-0.62	6.25 %	9	-0.59	6.25 %
	9	-0.61	6.25 %	6	-0.56	6.25 %
PSN	527	-3.00	18.16 %	234	-2.93	14.65 %
	496	-2.95	17.09 %	789	-2.91	17.58 %
	789	-2.88	10.55 %	527	-2.62	15.23 %
	234	-2.85	11.72 %	79	-2.61	7.32 %
	79	-2.70	7.03 %	496	-2.54	15.04 %
	229	-2.66	8.59 %	944	-2.51	4.59 %
	794	-2.65	10.74 %	794	-2.47	8.79 %
	944	-2.62	6.74 %	229	-2.46	8.11 %
	287	-2.23	2.15 %	287	-2.20	2.54 %
	736	-2.20	2.34 %	736	-2.17	2.54 %
	341	-2.09	2.83 %	906	-1.72	0.68 %
	117	-1.85	2.05 %	117	-1.72	0.68 %
				378	-1.64	1.07 %
				645	-1.63	1.17 %
RECN	28	-1.05	31.25 %	3	-1.12	37.50 %
	3	-1.03	28.12 %	28	-1.11	37.50 %
	9	-0.99	12.50 %	10	-0.96	6.25 %
	22	-0.99	12.50 %	9	-0.90	6.25 %
	21	-0.96	9.38 %	21	-0.89	6.25 %
	10	-0.96	6.25 %	22	-0.87	6.25 %

Basin states, their energy and cluster size. See Section A for details on state indexing.

Major basins are listed on first two rows (highlighted in purple) for each group and network. Unique basins are shaded in light purple. For each group, basins are sorted from lowest energy, and then from largest size.

Table C.2: Separate model: Basin characteristics (continued)

	Healthy			Depressed		
Network	B	E	Size	B	E	Size
SMN	3	-2.12	50.00 %	3	-1.99	50.00 %
	28	-2.09	50.00 %	28	-1.95	50.00 %
VDMN	206	-2.82	20.31 %	165	-2.94	23.44 %
	305	-2.75	19.73 %	346	-2.92	24.02 %
	338	-2.72	21.29 %	206	-2.75	20.90 %
	165	-2.72	21.68 %	305	-2.74	20.90 %
	99	-1.85	8.59 %	99	-1.77	5.08 %
	404	-1.83	8.40 %	404	-1.73	5.66 %
VSPN	85	-2.80	21.09 %	85	-2.81	26.17 %
	170	-2.76	21.09 %	170	-2.77	23.44 %
	204	-2.20	20.70 %	51	-2.12	17.19 %
	51	-2.19	20.70 %	204	-2.11	16.41 %
	102	-1.75	6.25 %	102	-1.80	6.25 %
	153	-1.74	6.25 %	153	-1.77	6.25 %
	15	-1.26	1.95 %	232	-1.71	2.73 %
	240	-1.24	1.95 %	240	-1.14	1.56 %

Basin states, their energy and cluster size. See Section A for details on state indexing.
Major basins are listed on first two rows (highlighted in purple) for each group and network. Unique basins are shaded in light purple. For each group, basins are sorted from lowest energy, and then from largest size.

Table C.3: Separate model: Major basins transition dynamics

Network	Score	Healthy	Depressed	p-value
AN	Traveling	0.91 ± 0.37	0.90 ± 0.39	
	Lingering	0.48 ± 0.06	0.49 ± 0.06	
	TR(A)	0.15 ± 0.04	0.15 ± 0.04	
	TR(P)	0.18 ± 0.04	0.18 ± 0.04	
	SR(A)	0.31 ± 0.09	0.31 ± 0.09	
	SR(P)	0.17 ± 0.07	0.17 ± 0.07	
ASN	Traveling	0.38 ± 0.23	0.40 ± 0.18	
	Lingering	0.41 ± 0.07	0.40 ± 0.08	
	TR(A)	0.08 ± 0.04	0.08 ± 0.03	
	TR(P)	0.21 ± 0.04	0.21 ± 0.04	
	SR(A)	0.09 ± 0.06	0.10 ± 0.06	*
	SR(P)	0.32 ± 0.10	0.29 ± 0.10	*
BGN	Traveling	0.78 ± 0.42	0.77 ± 0.34	
	Lingering	0.19 ± 0.08	0.21 ± 0.09	
	TR(A)	0.08 ± 0.03	0.08 ± 0.03	
	TR(P)	0.11 ± 0.03	0.11 ± 0.03	
	SR(A)	0.11 ± 0.07	0.12 ± 0.08	
	SR(P)	0.08 ± 0.03	0.09 ± 0.04	
DDMN	Traveling	0.09 ± 0.08	0.09 ± 0.09	
	Lingering	0.58 ± 0.06	0.54 ± 0.07	***
	TR(A)	0.02 ± 0.02	0.02 ± 0.02	
	TR(P)	0.24 ± 0.04	0.23 ± 0.04	*
	SR(A)	0.02 ± 0.02	0.02 ± 0.02	
	SR(P)	0.56 ± 0.07	0.53 ± 0.07	***
LN	Traveling	0.17 ± 0.11	0.15 ± 0.10	
	Lingering	0.38 ± 0.07	0.47 ± 0.08	***
	TR(A)	0.03 ± 0.02	0.03 ± 0.02	
	TR(P)	0.20 ± 0.04	0.23 ± 0.05	***
	SR(A)	0.03 ± 0.02	0.03 ± 0.03	
	SR(P)	0.35 ± 0.07	0.44 ± 0.08	***
LECN	Traveling	0.17 ± 0.09	0.16 ± 0.08	
	Lingering	0.53 ± 0.06	0.59 ± 0.05	***
	TR(A)	0.04 ± 0.02	0.04 ± 0.02	
	TR(P)	0.24 ± 0.03	0.27 ± 0.04	***
	SR(A)	0.04 ± 0.03	0.04 ± 0.03	
	SR(P)	0.49 ± 0.07	0.55 ± 0.07	***

Traveling scores (Equation 2.16) and *Lingering scores* (Equation 2.17) of individual participants on each group. *Traveling score* is based on the traveling rates between major basins ($TR(P)$) and their peripherals ($TR(A)$). *Lingering score* is based on the staying rates within major basins ($SR(A)$) and their peripherals ($SR(P)$).

$(*)$ $p < 0.05$; $(**)$ $p < 0.01$; $(***)$ $p < 0.005$; between-group, pairwise comparison of traveling/lingering scores using one-way ANOVA

Table C.3: Separate model: Major basins transition dynamics (continued)

Network	Score	Healthy	Depressed	p-value
PN	Traveling	0.83 ± 0.31	0.79 ± 0.28	
	Lingering	0.29 ± 0.07	0.29 ± 0.07	
	TR(A)	0.10 ± 0.03	0.09 ± 0.02	
	TR(P)	0.12 ± 0.03	0.13 ± 0.03	
	SR(A)	0.18 ± 0.07	0.17 ± 0.08	
	SR(P)	0.11 ± 0.04	0.12 ± 0.04	***
PSN	Traveling	0.05 ± 0.07	0.06 ± 0.09	
	Lingering	0.14 ± 0.06	0.13 ± 0.06	
	TR(A)	0.01 ± 0.01	0.01 ± 0.01	
	TR(P)	0.12 ± 0.04	0.09 ± 0.03	***
	SR(A)	0.00 ± 0.00	0.00 ± 0.01	***
	SR(P)	0.14 ± 0.06	0.13 ± 0.06	
RECN	Traveling	0.35 ± 0.18	0.30 ± 0.15	**
	Lingering	0.18 ± 0.06	0.30 ± 0.08	***
	TR(A)	0.04 ± 0.02	0.04 ± 0.02	
	TR(P)	0.13 ± 0.03	0.15 ± 0.03	***
	SR(A)	0.04 ± 0.03	0.04 ± 0.03	
	SR(P)	0.14 ± 0.05	0.26 ± 0.07	***
SMN	Traveling	0.37 ± 0.15	0.34 ± 0.14	
	Lingering	0.50 ± 0.06	0.50 ± 0.05	
	TR(A)	0.09 ± 0.03	0.08 ± 0.03	
	TR(P)	0.25 ± 0.04	0.26 ± 0.04	
	SR(A)	0.13 ± 0.07	0.11 ± 0.06	*
	SR(P)	0.36 ± 0.09	0.39 ± 0.08	*
VDMN	Traveling	0.08 ± 0.09	0.08 ± 0.10	
	Lingering	0.16 ± 0.06	0.24 ± 0.07	***
	TR(A)	0.01 ± 0.01	0.01 ± 0.01	
	TR(P)	0.12 ± 0.03	0.13 ± 0.03	***
	SR(A)	0.01 ± 0.01	0.01 ± 0.02	
	SR(P)	0.15 ± 0.06	0.23 ± 0.07	***
VSPN	Traveling	0.20 ± 0.14	0.17 ± 0.14	
	Lingering	0.17 ± 0.07	0.22 ± 0.07	***
	TR(A)	0.02 ± 0.02	0.02 ± 0.02	
	TR(P)	0.12 ± 0.03	0.13 ± 0.03	***
	SR(A)	0.02 ± 0.03	0.02 ± 0.03	
	SR(P)	0.14 ± 0.05	0.20 ± 0.06	***

Traveling scores (Equation 2.16) and *Lingering scores* (Equation 2.17) of individual participants on each group. *Traveling score* is based on the traveling rates between major basins ($TR(P)$) and their peripherals ($TR(A)$). *Lingering score* is based on the staying rates within major basins ($SR(A)$) and their peripherals ($SR(P)$).

$(*)$ $p < 0.05$; $(**)$ $p < 0.01$; $(***)$ $p < 0.005$; between-group, pairwise comparison of traveling/lingering scores using one-way ANOVA

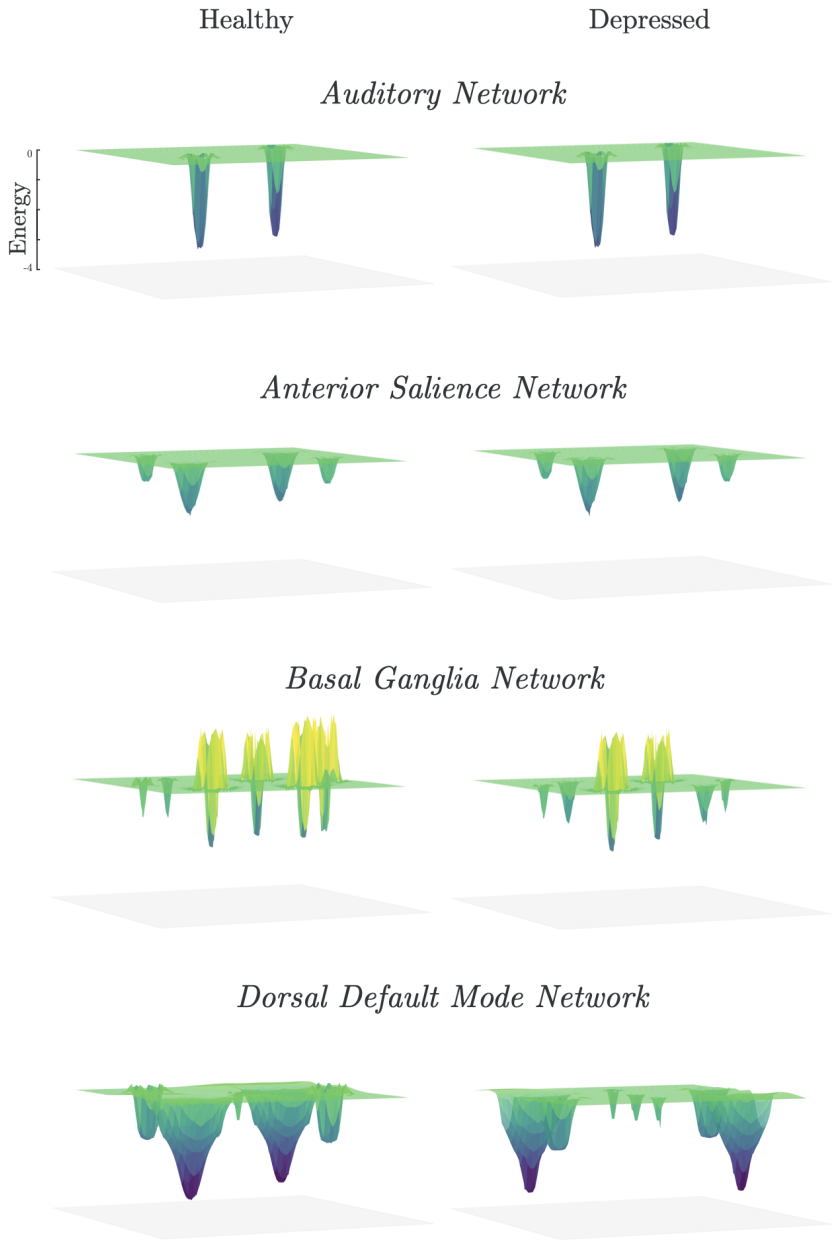

Figure C.1: Separate model: Energy landscapes

3D representations of energy landscapes across groups and networks. Basins and clusters are plotted on arbitrary state space; i.e. x- and y-locations are arbitrary. Basin sizes are proportional to the number of neighboring states clustered (Section 2.5). See Supplementary Table C.2 for detailed information on individual basins.

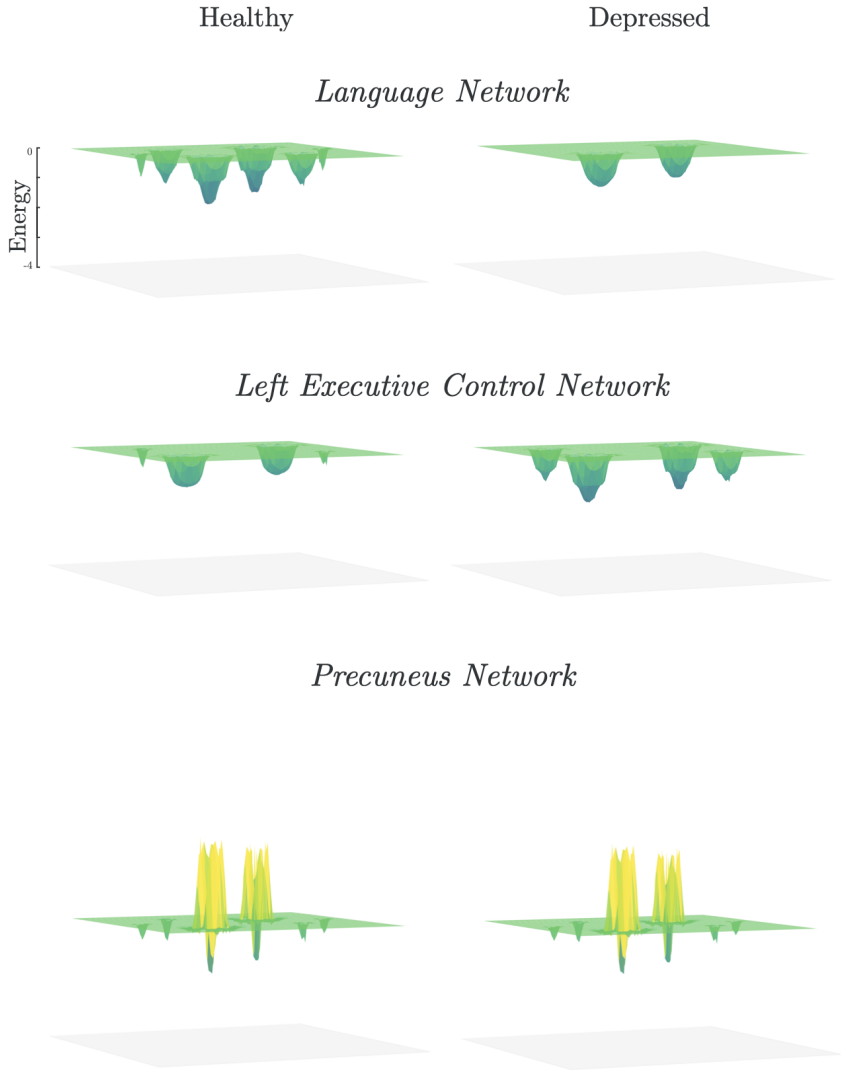

Figure C.1: Separate model: Energy landscapes (continued)

3D representations of energy landscapes across groups and networks. Basins and clusters are plotted on arbitrary state space; i.e. x- and y-locations are arbitrary. Basin sizes are proportional to the number of neighboring states clustered (Section 2.5). See Supplementary Table D.2 for detailed information on individual basins.

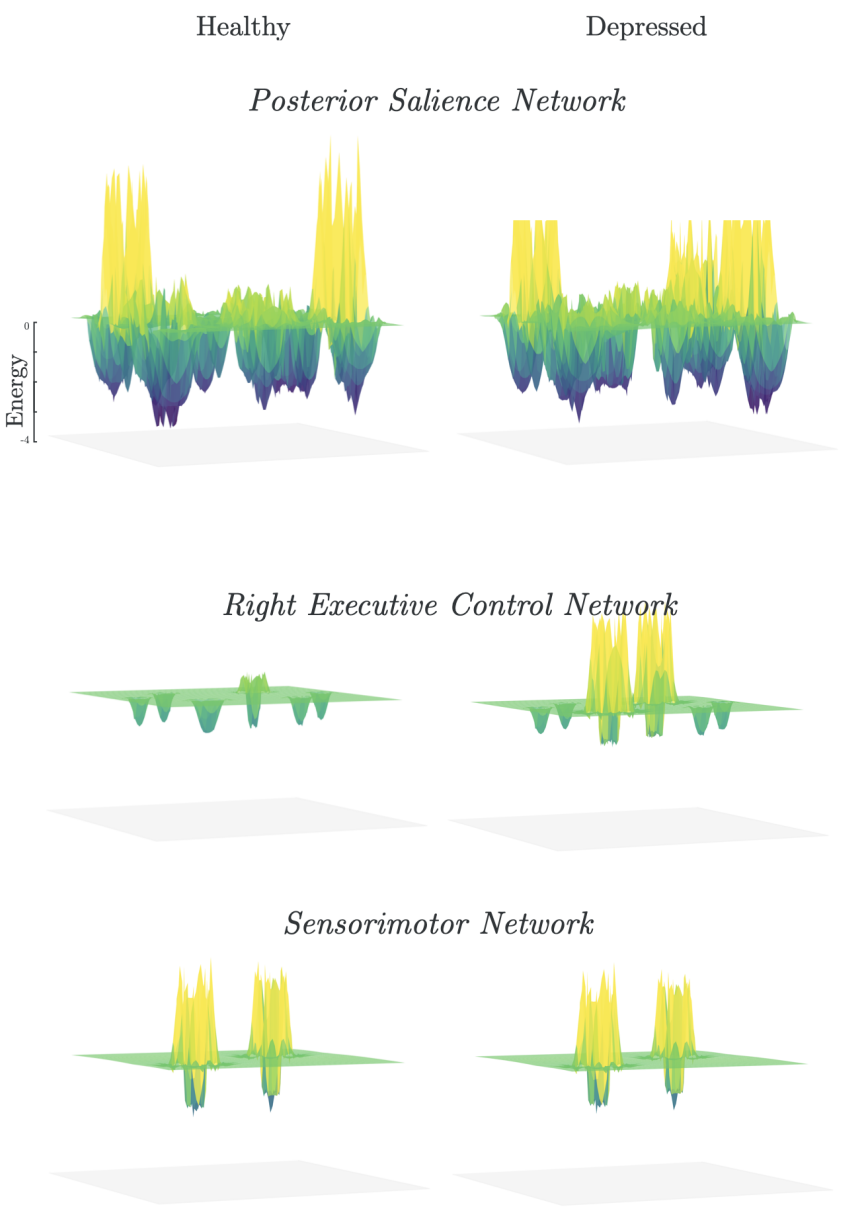

Figure C.1: Separate model: Energy landscapes (continued)

3D representations of energy landscapes across groups and networks. Basins and clusters are plotted on arbitrary state space; i.e. x- and y-locations are arbitrary. Basin sizes are proportional to the number of neighboring states clustered (Section 2.5). See Supplementary Table D.2 for detailed information on individual basins.

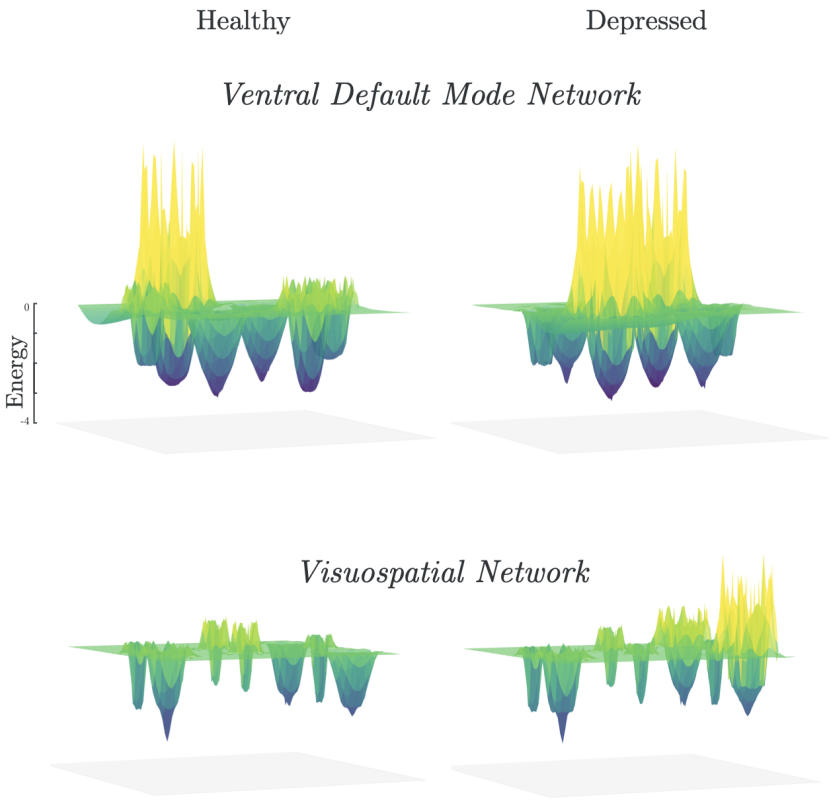

Figure C.1: Separate model: Energy landscapes (continued)

3D representations of energy landscapes across groups and networks. Basins and clusters are plotted on arbitrary state space; i.e. x- and y-locations are arbitrary. Basin sizes are proportional to the number of neighboring states clustered (Section 2.5). See Supplementary Table D.2 for detailed information on individual basins.

D Segregated Model Results

Complete results of energy landscape analyses for the segregated model framework (Section 5) are presented here. Analyses were conducted separately for each group (healthy, non-melancholic, and melancholic) and on each functional network (Table A.2).

Table D.1: Segregated model: Basin occurrence frequency

	Basin frequency			p-value					
Network	Healthy	Non-melancholic	Melancholic	(H, N)	(H, M)	(N, M)	KW[1]	Site[2]	G×S[3]
AN	0.64 ± 0.03	0.62 ± 0.02	0.60 ± 0.03		***	***	***	***	***
ASN	0.28 ± 0.01	0.31 ± 0.03	0.39 ± 0.04	***	***	***	***	***	***
BGN	0.59 ± 0.02	0.54 ± 0.02	0.63 ± 0.01	***	***	***	***	***	***
DDMN	0.05 ± 0.00	0.07 ± 0.01	0.11 ± 0.01	***	***	***	***	***	***
LN	0.23 ± 0.01	0.25 ± 0.01	0.20 ± 0.01	***	***	***	***	***	***
LECN	0.24 ± 0.02	0.15 ± 0.01	0.19 ± 0.03	***	***	***	***	***	***
PN	0.69 ± 0.01	0.63 ± 0.01	0.65 ± 0.03	***	***	***	***	***	***
PSN	0.09 ± 0.01	0.21 ± 0.04	0.10 ± 0.01	***	***	***	***	***	***
RECN	0.41 ± 0.01	0.34 ± 0.00	0.38 ± 0.01	***	***	***	***	***	***
SMN	0.44 ± 0.04	0.43 ± 0.02	0.30 ± 0.02		***	***	***	***	***
VDMN	0.06 ± 0.02	0.14 ± 0.01	0.09 ± 0.01	***	***	***	***	***	***
VSPN	0.13 ± 0.01	0.20 ± 0.01	0.20 ± 0.00	***	***	***	***	***	***

Occurrence frequency (mean ± std) of basins on individual participants' fMRI time signals.

(***) $p < 0.005$; between-group, pairwise comparison of basin frequencies using one-way ANOVA with Bonferroni correction

[1] Kruskal-Wallis test for non-normal distribution

[2] Two-way ANOVA test for significant differences across fMRI recording sites

[3] Two-way ANOVA test for significant interaction between group (H, N, M) and site (HUH, HRC, HKH, COI)

Table D.2: Segregated model: Basin characteristics

Network	Healthy B	Healthy E	Healthy Size	Non-melancholic B	Non-melancholic E	Non-melancholic Size	Melancholic B	Melancholic E	Melancholic Size
AN	1	-3.00	50.00 %	1	-3.03	50.00 %	1	-3.02	50.00 %
	6	-2.97	50.00 %	6	-2.99	50.00 %	6	-2.99	50.00 %
ASN	9	-1.78	43.75 %	9	-1.94	43.75 %	9	-1.91	43.75 %
	22	-1.74	43.75 %	22	-1.90	43.75 %	22	-1.91	43.75 %
	3	-0.85	6.25 %	3	-0.79	6.25 %	3	-0.94	6.25 %
	28	-0.83	6.25 %	28	-0.74	6.25 %	28	-0.92	6.25 %
BGN	6	-1.92	25.00 %	6	-2.03	28.12 %	6	-2.01	28.12 %
	25	-1.92	25.00 %	25	-2.00	28.12 %	25	-2.01	28.12 %
	26	-1.51	15.62 %	26	-1.60	12.50 %	26	-1.51	12.50 %
	28	-1.48	9.38 %	5	-1.60	12.50 %	5	-1.49	12.50 %
	3	-1.47	15.62 %	28	-1.38	9.38 %	28	-1.43	9.38 %
	5	-1.47	9.38 %	3	-1.34	9.38 %	3	-1.39	9.38 %
DDMN	279	-3.32	45.70 %	279	-3.15	50.59 %	279	-3.35	44.53 %
	232	-3.29	46.29 %	168	-3.13	48.05 %	232	-3.30	44.92 %
	340	-1.68	3.71 %	419	-1.20	0.59 %	340	-1.70	4.88 %
	171	-1.63	3.71 %	92	-1.08	0.78 %	139	-1.66	4.69 %
	419	-1.29	0.59 %				419	-1.25	0.59 %
							404	-1.13	0.39 %
LN	29	-1.51	37.50 %	34	-1.71	46.88 %	29	-1.46	43.75 %
	34	-1.51	37.50 %	29	-1.65	46.88 %	34	-1.45	43.75 %
	56	-1.19	10.94 %	56	-1.19	1.56 %	56	-1.14	6.25 %
	7	-1.19	10.94 %	7	-1.18	1.56 %	7	-1.11	6.25 %
	19	-0.95	1.56 %	19	-1.08	1.56 %			
	44	-0.93	1.56 %	44	-1.08	1.56 %			
LECN	28	-1.03	46.88 %	28	-1.11	50.00 %	28	-1.11	50.00 %
	3	-1.03	46.88 %	11	-1.10	46.88 %	3	-1.09	50.00 %
	5	-0.68	3.12 %	5	-0.69	3.12 %			
	26	-0.68	3.12 %						
PN	12	-1.49	37.50 %	3	-1.44	37.50 %	12	-1.44	37.50 %
	3	-1.43	37.50 %	12	-1.42	37.50 %	3	-1.41	37.50 %
	10	-0.87	6.25 %	10	-0.86	6.25 %	10	-0.81	6.25 %
	5	-0.81	6.25 %	5	-0.70	6.25 %	5	-0.80	6.25 %
	6	-0.62	6.25 %	6	-0.62	6.25 %	9	-0.60	6.25 %
	9	-0.61	6.25 %	9	-0.60	6.25 %	6	-0.54	6.25 %

Basin states, their energy and cluster size. See Section A for details on state indexing.
Major basins are listed on first two rows (highlighted in purple) for each group and network. Unique basins are shaded in light purple. For each group, basins are sorted from lowest energy, and then from largest size.

Table D.2: Segregated model: Basin characteristics (continued)

Network	Healthy			Non-melancholic			Melancholic		
	B	E	Size	B	E	Size	B	E	Size
PSN	527	-3.00	18.16 %	789	-2.97	13.38 %	234	-2.93	16.50 %
	496	-2.95	17.09 %	234	-2.95	13.38 %	789	-2.90	17.19 %
	789	-2.88	10.55 %	79	-2.93	15.23 %	15	-2.64	20.70 %
	234	-2.85	11.72 %	944	-2.87	14.55 %	1008	-2.49	20.02 %
	79	-2.70	7.03 %	527	-2.81	8.01 %	794	-2.42	8.40 %
	229	-2.66	8.59 %	496	-2.77	7.91 %	229	-2.40	7.71 %
	794	-2.65	10.74 %	794	-2.68	11.13 %	287	-2.17	2.54 %
	944	-2.62	6.74 %	229	-2.68	10.94 %	736	-2.14	3.61 %
	287	-2.23	2.15 %	287	-2.35	1.46 %	378	-1.79	1.37 %
	736	-2.20	2.34 %	736	-2.32	1.37 %	906	-1.71	0.98 %
	341	-2.09	2.83 %	714	-1.98	1.17 %	117	-1.71	0.98 %
	117	-1.85	2.05 %	309	-1.95	1.46 %			
RECN	28	-1.05	31.25 %	28	-1.13	31.25 %	12	-1.12	37.50 %
	3	-1.03	28.12 %	3	-1.13	28.12 %	3	-1.11	37.50 %
	9	-0.99	12.50 %	10	-1.12	12.50 %	10	-0.90	6.25 %
	22	-0.99	12.50 %	21	-1.00	12.50 %	9	-0.86	6.25 %
	21	-0.96	9.38 %	9	-0.99	6.25 %	21	-0.86	6.25 %
	10	-0.96	6.25 %	22	-0.97	9.38 %	22	-0.84	6.25 %
SMN	3	-2.12	50.00 %	3	-1.97	53.12 %	3	-2.00	50.00 %
	28	-2.09	50.00 %	28	-1.92	46.88 %	28	-1.96	50.00 %
VDMN	206	-2.82	20.31 %	206	-2.91	21.09 %	346	-3.03	25.20 %
	305	-2.75	19.73 %	305	-2.82	17.77 %	165	-3.03	24.02 %
	338	-2.72	21.29 %	338	-2.66	20.31 %	305	-2.71	19.73 %
	165	-2.72	21.68 %	165	-2.66	23.63 %	206	-2.70	21.29 %
	99	-1.85	8.59 %	99	-2.01	8.01 %	99	-1.69	5.08 %
	404	-1.83	8.40 %	412	-1.95	9.18 %	404	-1.67	4.69 %
VSPN	85	-2.80	21.09 %	170	-2.85	29.30 %	85	-2.79	26.56 %
	170	-2.76	21.09 %	85	-2.85	28.12 %	170	-2.74	23.83 %
	204	-2.20	20.70 %	51	-2.22	14.06 %	204	-2.10	17.19 %
	51	-2.19	20.70 %	204	-2.14	14.06 %	51	-2.09	16.80 %
	102	-1.75	6.25 %	102	-1.57	6.25 %	102	-1.88	6.25 %
	153	-1.74	6.25 %	153	-1.51	6.25 %	153	-1.86	6.25 %
	15	-1.26	1.95 %	240	-1.16	1.56 %	232	-1.76	2.73 %
	240	-1.24	1.95 %	15	-1.12	0.39 %	240	-1.13	0.39 %

Basin states, their energy and cluster size. See Section A for details on state indexing.

Major basins are listed on first two rows (highlighted in purple) for each group and network. Unique basins are shaded in light purple. For each group, basins are sorted from lowest energy, and then from largest size.

Table D.3: Segregated model: Major basins transition dynamics

Network	Score	Healthy	Non-melancholic	Melancholic	p-value (H,N)	(H,M)	(N,M)	KW
AN	Traveling	0.91 ± 0.37	0.85 ± 0.29	0.92 ± 0.41				
	Lingering	0.48 ± 0.06	0.47 ± 0.07	0.49 ± 0.06				
	TR(A)	0.15 ± 0.04	0.15 ± 0.04	0.15 ± 0.04				
	TR(P)	0.18 ± 0.04	0.19 ± 0.04	0.18 ± 0.04				
	SR(A)	0.31 ± 0.09	0.31 ± 0.09	0.31 ± 0.09				
	SR(P)	0.17 ± 0.07	0.16 ± 0.05	0.18 ± 0.08				
ASN	Traveling	0.38 ± 0.23	0.41 ± 0.18	0.39 ± 0.18				
	Lingering	0.41 ± 0.07	0.38 ± 0.08	0.40 ± 0.08				
	TR(A)	0.08 ± 0.04	0.08 ± 0.04	0.08 ± 0.03				
	TR(P)	0.21 ± 0.04	0.21 ± 0.04	0.21 ± 0.04				
	SR(A)	0.09 ± 0.06	0.10 ± 0.06	0.10 ± 0.06				*
	SR(P)	0.32 ± 0.10	0.28 ± 0.11	0.30 ± 0.10				*
BGN	Traveling	0.78 ± 0.42	0.82 ± 0.35	0.75 ± 0.33				
	Lingering	0.19 ± 0.08	0.19 ± 0.08	0.21 ± 0.09				
	TR(A)	0.08 ± 0.03	0.09 ± 0.03	0.07 ± 0.03				
	TR(P)	0.11 ± 0.03	0.11 ± 0.03	0.11 ± 0.03				
	SR(A)	0.11 ± 0.07	0.12 ± 0.07	0.12 ± 0.08				
	SR(P)	0.08 ± 0.03	0.08 ± 0.03	0.09 ± 0.04				
DDMN	Traveling	0.09 ± 0.08	0.05 ± 0.06	0.10 ± 0.09			*	*
	Lingering	0.58 ± 0.06	0.63 ± 0.05	0.55 ± 0.07	***	**	***	***
	TR(A)	0.02 ± 0.02	0.01 ± 0.01	0.02 ± 0.02				
	TR(P)	0.24 ± 0.04	0.28 ± 0.05	0.23 ± 0.04	***		***	***
	SR(A)	0.02 ± 0.02	0.01 ± 0.01	0.02 ± 0.02				
	SR(P)	0.56 ± 0.07	0.62 ± 0.05	0.53 ± 0.07	***	***	***	***
LN	Traveling	0.17 ± 0.11	0.15 ± 0.10	0.14 ± 0.09				
	Lingering	0.38 ± 0.07	0.48 ± 0.08	0.48 ± 0.07	***	***		***
	TR(A)	0.03 ± 0.02	0.04 ± 0.02	0.03 ± 0.02				
	TR(P)	0.20 ± 0.04	0.24 ± 0.05	0.23 ± 0.04	***	***		***
	SR(A)	0.03 ± 0.02	0.03 ± 0.02	0.03 ± 0.03				
	SR(P)	0.35 ± 0.07	0.46 ± 0.09	0.45 ± 0.08	***	***		***
LECN	Traveling	0.17 ± 0.09	0.14 ± 0.08	0.17 ± 0.08				
	Lingering	0.53 ± 0.06	0.55 ± 0.06	0.61 ± 0.06		***	***	***
	TR(A)	0.04 ± 0.02	0.04 ± 0.02	0.04 ± 0.02				
	TR(P)	0.24 ± 0.03	0.25 ± 0.04	0.26 ± 0.04		***		***
	SR(A)	0.04 ± 0.03	0.04 ± 0.03	0.04 ± 0.03				
	SR(P)	0.49 ± 0.07	0.51 ± 0.07	0.57 ± 0.07		***	***	***

Traveling scores (Equation 2.16) and *Lingering scores* (Equation 2.17) of individual participants on each group. *Traveling score* is based on the traveling rates between major basins ($TR(P)$) and their peripherals ($TR(A)$). *Lingering score* is based on the staying rates within major basins ($SR(A)$) and their peripherals ($SR(P)$).

$(*)$ $p < 0.05$; $(**)$ $p < 0.01$; $(***)$ $p < 0.005$; between-group, pairwise comparison of traveling/lingering scores using one-way ANOVA with Bonferroni correction.

$(*)$ $p < 0.05$; $(**)$ $p < 0.01$; $(***)$ $p < 0.005$; Kruskal-Wallis test for non-normal distribution

Table D.3: Segregated model: Major basins transition dynamics (continued)

Network	Score	Healthy	Non-melancholic	Melancholic	p-value (H,N)	(H,M)	(N,M)	KW
PSN	Traveling	0.05 ± 0.07	0.08 ± 0.14	0.05 ± 0.07				
	Lingering	0.14 ± 0.06	0.09 ± 0.05	0.14 ± 0.07	***		***	***
	TR(A)	0.01 ± 0.01	0.01 ± 0.01	0.00 ± 0.01				
	TR(P)	0.12 ± 0.04	0.08 ± 0.02	0.10 ± 0.03	***	***	***	***
	SR(A)	0.00 ± 0.00	0.01 ± 0.01	0.00 ± 0.01	***			
	SR(P)	0.14 ± 0.06	0.09 ± 0.04	0.13 ± 0.06	***		***	***
PN	Traveling	0.83 ± 0.31	0.81 ± 0.29	0.78 ± 0.27				
	Lingering	0.29 ± 0.07	0.29 ± 0.07	0.30 ± 0.07				
	TR(A)	0.10 ± 0.03	0.09 ± 0.02	0.09 ± 0.02				
	TR(P)	0.12 ± 0.03	0.12 ± 0.03	0.13 ± 0.03				
	SR(A)	0.18 ± 0.07	0.16 ± 0.07	0.17 ± 0.08				
	SR(P)	0.11 ± 0.04	0.12 ± 0.04	0.12 ± 0.04		*		**
RECN	Traveling	0.35 ± 0.18	0.37 ± 0.18	0.25 ± 0.11		***	***	***
	Lingering	0.18 ± 0.06	0.20 ± 0.07	0.31 ± 0.06		***	***	***
	TR(A)	0.04 ± 0.02	0.05 ± 0.02	0.04 ± 0.02				
	TR(P)	0.13 ± 0.03	0.13 ± 0.03	0.15 ± 0.03		***	***	***
	SR(A)	0.04 ± 0.03	0.04 ± 0.03	0.05 ± 0.03		*		*
	SR(P)	0.14 ± 0.05	0.16 ± 0.06	0.27 ± 0.05		***	***	***
SMN	Traveling	0.37 ± 0.15	0.35 ± 0.16	0.33 ± 0.13				
	Lingering	0.50 ± 0.06	0.49 ± 0.06	0.51 ± 0.05				
	TR(A)	0.09 ± 0.03	0.09 ± 0.03	0.08 ± 0.03				
	TR(P)	0.25 ± 0.04	0.26 ± 0.04	0.25 ± 0.04				
	SR(A)	0.13 ± 0.07	0.12 ± 0.07	0.11 ± 0.06				
	SR(P)	0.36 ± 0.09	0.38 ± 0.10	0.39 ± 0.08		*		
VDMN	Traveling	0.08 ± 0.09	0.11 ± 0.14	0.09 ± 0.10				
	Lingering	0.16 ± 0.06	0.15 ± 0.05	0.26 ± 0.07		***	***	***
	TR(A)	0.01 ± 0.01	0.01 ± 0.01	0.01 ± 0.01				
	TR(P)	0.12 ± 0.03	0.11 ± 0.03	0.14 ± 0.03		***	***	***
	SR(A)	0.01 ± 0.01	0.01 ± 0.01	0.01 ± 0.02				
	SR(P)	0.15 ± 0.06	0.14 ± 0.05	0.25 ± 0.07		***	***	***
VSPN	Traveling	0.20 ± 0.14	0.17 ± 0.13	0.17 ± 0.14				
	Lingering	0.17 ± 0.07	0.26 ± 0.07	0.22 ± 0.07	***	***	*	***
	TR(A)	0.02 ± 0.02	0.03 ± 0.02	0.02 ± 0.02				
	TR(P)	0.12 ± 0.03	0.16 ± 0.03	0.13 ± 0.03	***	**	***	***
	SR(A)	0.02 ± 0.03	0.02 ± 0.03	0.02 ± 0.03				
	SR(P)	0.14 ± 0.05	0.24 ± 0.06	0.20 ± 0.06	***	***	**	***

Traveling scores (Equation 2.16) and *Lingering scores* (Equation 2.17) of individual participants on each group. *Traveling score* is based on the traveling rates between major basins ($TR(P)$) and their peripherals ($TR(A)$). *Lingering score* is based on the staying rates within major basins ($SR(A)$) and their peripherals ($SR(P)$).

$(*)$ $p < 0.05$; $(**)$ $p < 0.01$; $(***)$ $p < 0.005$; between-group, pairwise comparison of traveling/lingering scores using one-way ANOVA with Bonferroni correction.

$(*)$ $p < 0.05$; $(**)$ $p < 0.01$; $(***)$ $p < 0.005$; Kruskal-Wallis test for non-normal distribution

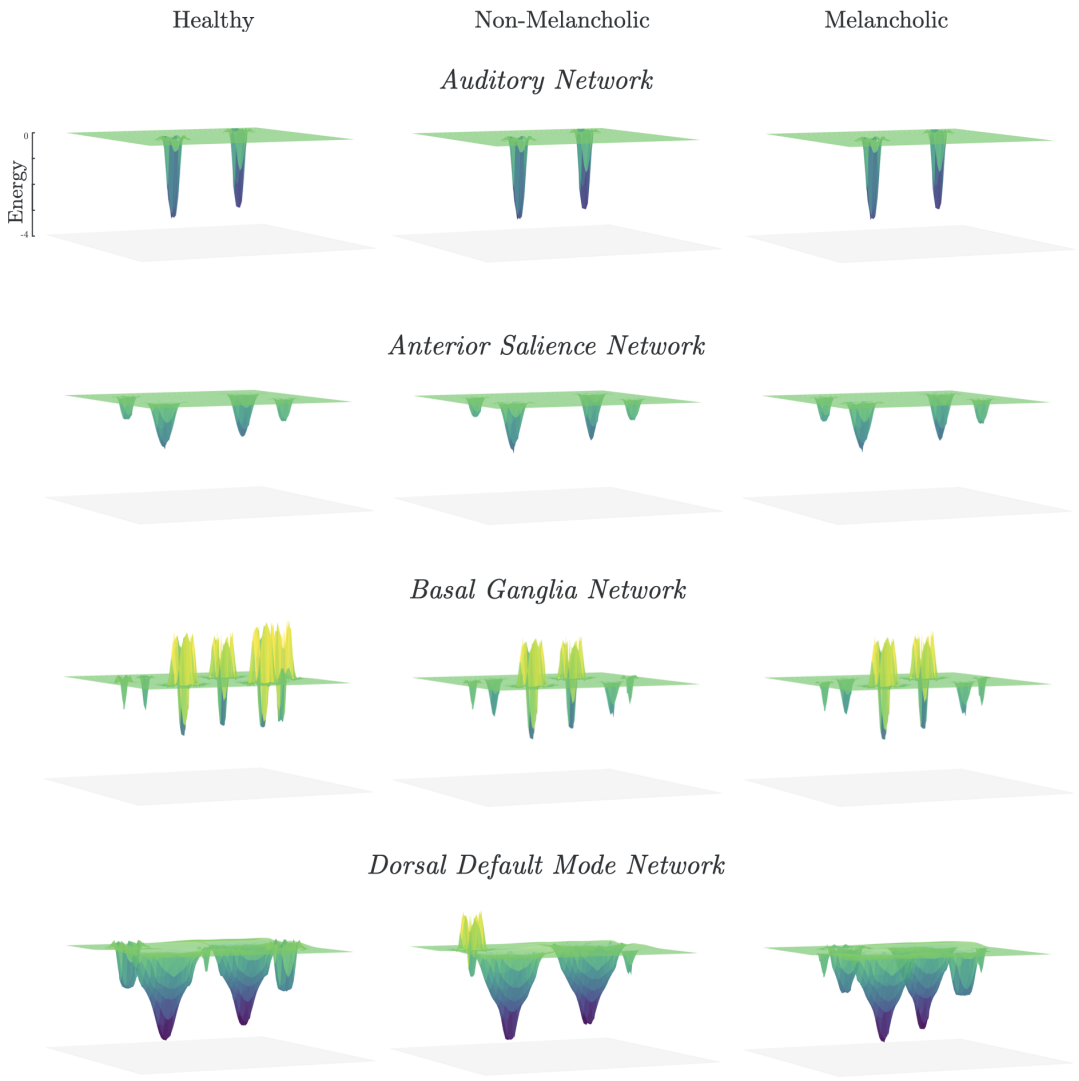

Figure D.1: Segregated model: Energy landscapes

3D representations of energy landscapes across groups and networks. Basins and clusters are plotted on arbitrary state space; i.e. x- and y-locations are arbitrary. Basin sizes are proportional to the number of neighboring states clustered (Section 2.5). See Supplementary Table D.2 for detailed information on individual basins.

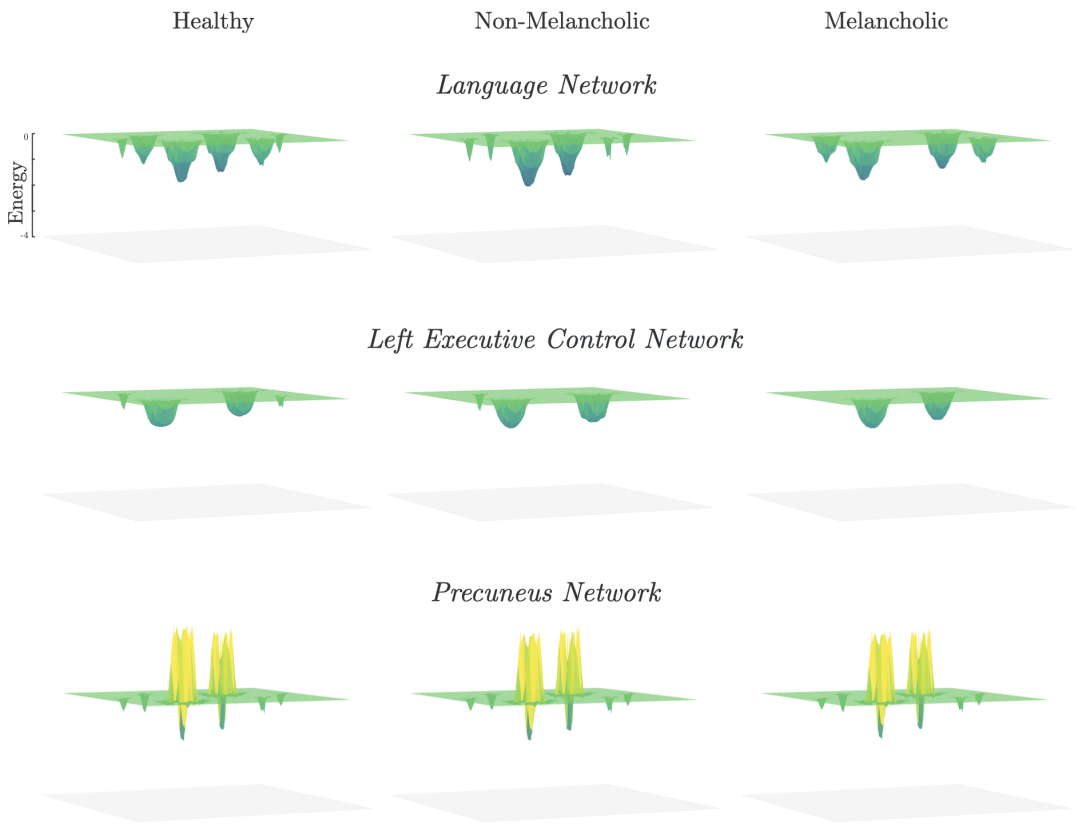

Figure D.1: Segregated model: Energy landscapes (continued)

3D representations of energy landscapes across groups and networks. Basins and clusters are plotted on arbitrary state space; i.e. x- and y-locations are arbitrary. Basin sizes are proportional to the number of neighboring states clustered (Section 2.5). See Supplementary Table D.2 for detailed information on individual basins.

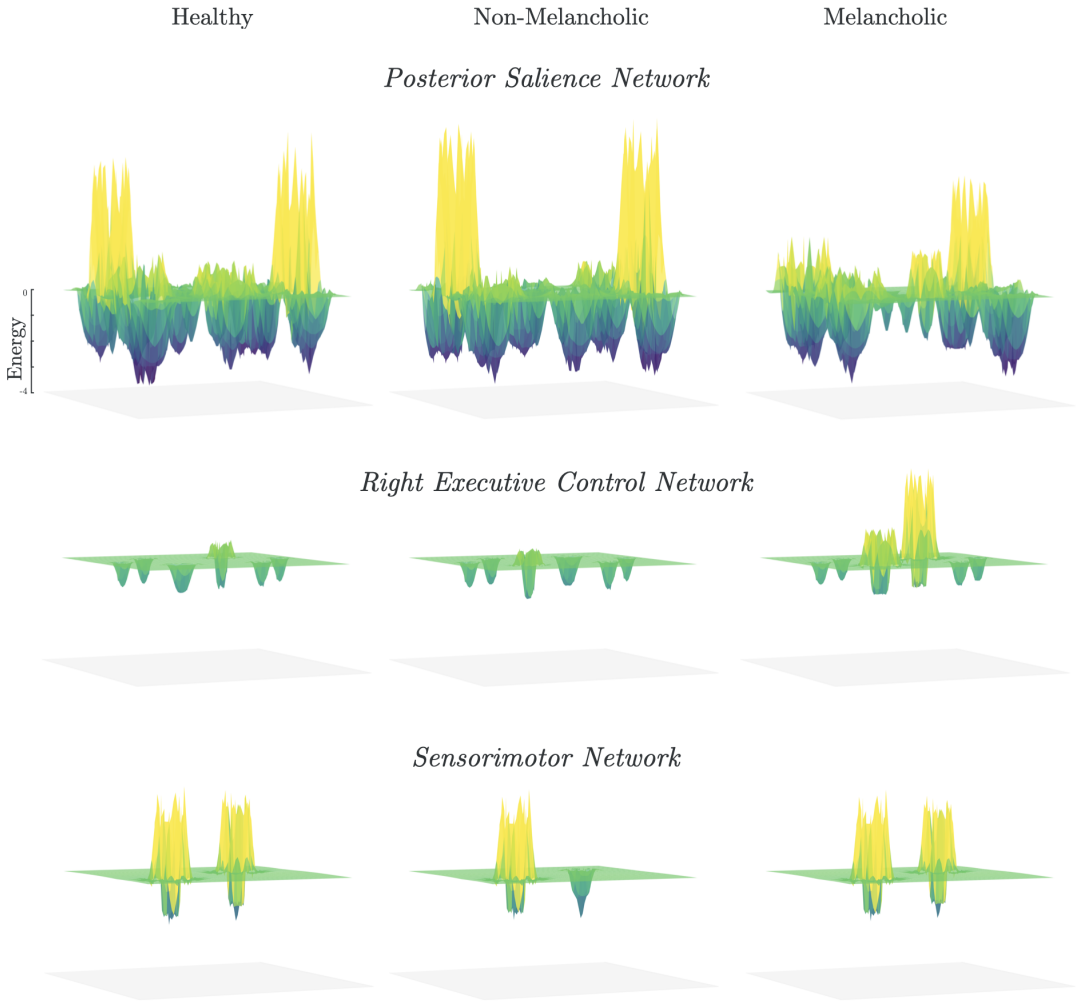

Figure D.1: Segregated model: Energy landscapes (continued)

3D representations of energy landscapes across groups and networks. Basins and clusters are plotted on arbitrary state space; i.e. x- and y-locations are arbitrary. Basin sizes are proportional to the number of neighboring states clustered (Section 2.5). See Supplementary Table D.2 for detailed information on individual basins.

Bibliography

[1] K. Davison. "Historical aspects of mood disorders". In: *Psychiatry* 5.4 (2006), pp. 115–118.

[2] P. Gilbert. *Depression: from psychology to brain state*. Lawrence Erlbaum Associates Ltd., 1984.

[3] E. S. Paykel. "Basic concepts of depression". In: *Dialogues in Clinical Neuroscience* 10.3 (2008), pp. 279–289.

[4] M. J. Tacchi and J. Scott. *Depression: A very short introduction*. Oxford University Press, 2017.

[5] Hippocrates et al. *Hippocrates*. Harvard University Press, 1923.

[6] K. A. Stewart. "Chapter 7 The Diseases Caused by Black Bile". In: *Galen's theory of black bile*. Brill, 2019, pp. 129–130.

[7] E. J. Engstrom. "Tempering madness: Emil Kraepelin's research on affective disorders". In: *Osiris* 31.1 (2016), pp. 163–180.

[8] S. Freud. "Mourning and Melancholia". In: *The Standard Edition of the Complete Psychological Works of Sigmund Freud*. Vol. 14. Hogarth Press, 1917, pp. 237–258.

[9] A. J. Lewis. "Melancholia: A historical review". In: *Journal of Mental Science* 80.328 (1934), pp. 1–42.

[10] *Diagnostic and statistical manual of mental disorders: DSM-5*. American Psychiatric Association, 2017.

[11] A. Beck, R. Steer, and G. Brown. *BDI-II, Beck depression inventory: Manual*. Harcourt Brace, 1996, pp. 1–38.

[12] D. Sheehan et al. “The Mini-International Neuropsychiatric Interview (M.I.N.I.): the development and validation of a structured diagnostic psychiatric interview for DSM-IV and ICD-10”. In: *The Journal of Clinical Psychiatry* 59 (1998), pp. 34–57.

[13] E. I. Fried and R. M. Nesse. “Depression sum-scores don’t add up: why analyzing specific depression symptoms is essential”. In: *BMC Medicine* 13.1 (2015).

[14] E. Fried. “Moving forward: how depression heterogeneity hinders progress in treatment and research”. In: *Expert Review of Neurotherapeutics* 17.5 (2017), pp. 423–425.

[15] D. A. Regier, E. A. Kuhl, and D. J. Kupfer. “The DSM-5: Classification and criteria changes”. In: *World Psychiatry* 12.2 (2013), pp. 92–98.

[16] A. T. Drysdale et al. “Resting-state connectivity biomarkers define neurophysiological subtypes of depression”. In: *Nature Medicine* 23.1 (2016), pp. 28–38.

[17] C. H. Fu, H. Steiner, and S. G. Costafreda. “Predictive neural biomarkers of clinical response in depression: A meta-analysis of functional and structural neuroimaging studies of pharmacological and psychological therapies”. In: *Neurobiology of Disease* 52 (2013), pp. 75–83.

[18] D. Goldberg. “The heterogeneity of “major depression””. In: *World Psychiatry* 10.3 (2011), pp. 226–228.

[19] C. J. Lynch, F. M. Gunning, and C. Liston. “Causes and Consequences of Diagnostic Heterogeneity in Depression: Paths to Discovering Novel Biological Depression Subtypes”. In: *Biological Psychiatry* 88.1 (2020), pp. 83–94.

[20] R. Strawbridge, A. H. Young, and A. J. Cleare. “Biomarkers for depression: recent insights, current challenges and future prospects”. In: *Neuropsychiatric Disease and Treatment* Volume 13 (2017), pp. 1245–1262.

[21] T. Wise et al. “Diagnostic and therapeutic utility of neuroimaging in depression: an overview”. In: *Neuropsychiatric Disease and Treatment* (2014), p. 1509.

[22] M. A. Davis, S. Eldridge, and C. Louden. “Biomarkers: Discovery, qualification, and application”. In: *Haschek and Rousseaux’s Handbook of Toxicologic Pathology* (2013), pp. 459–490.

[23] R. Haapakoski et al. “Cumulative meta-analysis of interleukins 6 and 1β, tumour necrosis factor α and C-reactive protein in patients with major depressive disorder”. In: *Brain, Behavior, and Immunity* 49 (2015), pp. 206–215.

[24] M. L. Molendijk et al. “Serum BDNF concentrations as peripheral manifestations of depression: Evidence from a systematic review and meta-analyses on 179 associations”. In: *Molecular Psychiatry* 19.7 (2013), pp. 791–800.

[25] F. Lamers et al. “Evidence for a differential role of HPA-axis function, inflammation and metabolic syndrome in melancholic versus atypical depression”. In: *Molecular Psychiatry* 18.6 (2012), pp. 692–699.

[26] J. Kaufman et al. “The 5-HT1A receptor in major depressive disorder”. In: *European Neuropsychopharmacology* 26.3 (2016), pp. 397–410.

[27] V. Menon and S. Crottaz-Herbette. “Combined EEG and fMRI studies of Human Brain Function”. In: *International Review of Neurobiology* (2005), pp. 291–321.

[28] J. C. Gore. “Principles and practice of functional MRI of the human brain”. In: *Journal of Clinical Investigation* 112.1 (2003), pp. 4–9.

[29] E. E. Bernstein, A. Heeren, and R. J. McNally. “Unpacking rumination and Executive control: A network perspective”. In: *Clinical Psychological Science* 5.5 (2017), pp. 816–826.

[30] K. Helm et al. “Neuronal connectivity in major depressive disorder: A systematic review”. In: *Neuropsychiatric Disease and Treatment* Volume 14 (2018), pp. 2715–2737.

[31] R. H. Kaiser et al. “Large-Scale Network Dysfunction in Major Depressive Disorder”. In: *JAMA Psychiatry* 72.6 (2015), p. 603.

[32] B. J. Li et al. “A brain network model for depression: From symptom understanding to disease intervention”. In: *CNS Neuroscience & Therapeutics* 24.11 (2018), pp. 1004–1019.

[33] H. Lv et al. “Resting-state functional MRI: Everything that nonexperts have always wanted to know”. In: *American Journal of Neuroradiology* (2018).

[34] P. C. Mulders et al. “Resting-state functional connectivity in major depressive disorder: A review”. In: *Neuroscience & Biobehavioral Reviews* 56 (2015), pp. 330–344.

[35] E. Rzepa and C. McCabe. “Anhedonia and depression severity dissociated by dmPFC resting-state functional connectivity in adolescents”. In: *Journal of Psychopharmacology* 32.10 (2018), pp. 1067–1074.

[36] E. Rzepa and C. McCabe. “Decreased anticipated pleasure correlates with increased salience network resting state functional connectivity in adolescents with depressive symptomatology”. In: *Journal of Psychiatric Research* 82 (2016), pp. 40–47.

[37] T. Watanabe et al. “A pairwise maximum entropy model accurately describes resting-state human brain networks”. In: *Nature Communications* 4.1 (2013).

[38] X.-N. Zuo et al. “Network centrality in the human functional connectome”. In: *Cerebral Cortex* 22.8 (2011), pp. 1862–1875.

[39] G. Deco, M. Senden, and V. Jirsa. “How anatomy shapes dynamics: A semi-analytical study of the brain at rest by a simple spin model”. In: *Frontiers in Computational Neuroscience* 6 (2012).

[40] E. Schneidman et al. “Weak pairwise correlations imply strongly correlated network states in a neural population”. In: *Nature* 440.7087 (2006), pp. 1007–1012.

[41] A. Ashourvan et al. “The energy landscape underpinning module dynamics in the human brain connectome”. In: *NeuroImage* 157 (2017), pp. 364–380.

[42] T. Ezaki et al. “Energy landscape analysis of neuroimaging data”. In: *Philosophical Transactions of the Royal Society A: Mathematical, Physical and Engineering Sciences* 375.2096 (2017), p. 20160287.

[43] T. Ezaki et al. “Age-related changes in the ease of dynamical transitions in human brain activity”. In: *Human Brain Mapping* 39.6 (2018), pp. 2673–2688.

[44] S. Gu et al. “The Energy Landscape of Neurophysiological Activity Implicit in Brain Network Structure”. In: *Scientific Reports* 8.1 (2018).

[45] T. Watanabe et al. “Energy landscape and dynamics of brain activity during human bistable perception”. In: *Nature Communications* 5.1 (2014).

[46] J. Kang, C. Pae, and H.-J. Park. “Energy landscape analysis of the subcortical brain network unravels system properties beneath resting state dynamics”. In: *NeuroImage* 149 (2017), pp. 153–164.

[47] A. M. Hayes et al. “Network destabilization and transition in depression: New methods for studying the dynamics of therapeutic change”. In: *Clinical Psychology Review* 41 (2015), pp. 27–39.

[48] P. E. Holtzheimer and H. S. Mayberg. “Stuck in a rut: rethinking depression and its treatment”. In: *Trends in Neurosciences* 34.1 (2011), pp. 1–9.

[49] R. J. Thompson et al. “The everyday emotional experience of adults with major depressive disorder: Examining emotional instability, inertia, and reactivity.” In: *Journal of Abnormal Psychology* 121.4 (2012), pp. 819–829.

[50] T. Nakano et al. “Enhancing Multi-Center Generalization of Machine Learning-Based Depression Diagnosis From Resting-State fMRI”. In: *Frontiers in Psychiatry* 11 (2020).

[51] T. Otsubo et al. “Reliability and validity of Japanese version of the MINI-international neuropsychiatric interview”. In: *Psychiatry and Clinical Neurosciences* 59.5 (2005), pp. 517–526.

[52] K. Smith. “Brain imaging: Fmri 2.0”. In: *Nature* 484.7392 (2012), pp. 24–26.

[53] M. D. Fox. “Clinical applications of resting state functional connectivity”. In: *Frontiers in Systems Neuroscience* (2010).

[54] F. A. Nasrallah et al. “Dependence of bold signal fluctuation on Arterial Blood CO2 and O2: Implication for resting-state functional connectivity”. In: *NeuroImage* 117 (2015), pp. 29–39.

[55] N. Yahata et al. “A small number of abnormal brain connections predicts adult autism spectrum disorder”. In: *Nature Communications* 7.1 (2016).

[56] J. D. Power et al. “Methods to detect, characterize, and remove motion artifact in resting state fMRI”. In: *NeuroImage* 84 (2014), pp. 320–341.

[57] J. D. Power, B. L. Schlaggar, and S. E. Petersen. “Recent progress and outstanding issues in motion correction in resting state fMRI”. In: *NeuroImage* 105 (2015), pp. 536–551.

[58] J. D. Power et al. “Spurious but systematic correlations in functional connectivity MRI networks arise from subject motion”. In: *NeuroImage* 59.3 (2012), pp. 2142–2154.

[59] W. R. Shirer et al. “Decoding Subject-Driven Cognitive States with Whole-Brain Connectivity Patterns”. In: *Cerebral Cortex* 22.1 (2011), pp. 158–165.

[60] T. Tokuda et al. “Identification of depression subtypes and relevant brain regions using a data-driven approach”. In: *Scientific Reports* 8.1 (2018).

[61] T. Watanabe and G. Rees. “Brain Network Dynamics in high-functioning individuals with autism”. In: *Nature Communications* 8.1 (2017).

[62] N. K. Logothetis et al. “Neurophysiological investigation of the basis of the fmri signal”. In: *Nature* 412.6843 (2001), pp. 150–157.

[63] A. Tang et al. “A maximum entropy model applied to spatial and temporal correlations from cortical networks in vitro”. In: *Journal of Neuroscience* 28.2 (2008), pp. 505–518.

[64] D. McQuarrie. *Statistical mechanics*. Harper & Row, 1973.

[65] J. Kang, C. Pae, and H.-J. Park. “Graph-theoretical analysis for energy landscape reveals the organization of state transitions in the resting-state human cerebral cortex”. In: *PLOS ONE* 14.9 (2019).

[66] B. D. W. Group. “Biomarkers and surrogate endpoints: Preferred definitions and Conceptual Framework”. In: *Clinical Pharmacology & Therapeutics* 69.3 (2001), pp. 89–95.

[67] Eickhoff, S.B. and Müller, V.I. “Functional connectivity”. In: *Brain Mapping* (2015), pp. 187–201.

[68] G. Chen et al. “Negative functional connectivity and its dependence on the shortest path length of positive network in the resting-state human brain”. In: *Brain Connectivity* 1.3 (2011), pp. 195–206.

[69] S. Ohmae. “The difference between depression and melancholia: two distinct conditions that were combined into a single category in DSM-III”. In: *Seishin Shinkeigaku Zasshi* 8 (2012), pp. 886–905.

[70] G. Parker et al. “Issues for DSM-5: Whither Melancholia? The Case for Its Classification as a Distinct Mood Disorder”. In: *American Journal of Psychiatry* 167.7 (2010), pp. 745–747.

[71] M. L. Crismon et al. “The Texas Medication Algorithm Project”. In: *The Journal of Clinical Psychiatry* 60.3 (1999), pp. 142–156.

[72] B. N. Gaynes et al. “What Did STAR*D Teach Us? Results From a Large-Scale, Practical, Clinical Trial for Patients With Depression”. In: *Psychiatric Services* 60.11 (2009), pp. 1439–1445.

[73] K. Fletcher et al. “Anhedonia in melancholic and non-melancholic depressive disorders”. In: *Journal of Affective Disorders* 184 (2015), pp. 81–88.

[74] M. Gili et al. “Clinical Patterns and Treatment Outcome in Patients with Melancholic, Atypical and Non-Melancholic Depressions”. In: *PLoS ONE* 7.10 (2012).

[75] M. Zimmerman. “Diagnostic Criteria for Melancholia: The Comparative Validity of DSM-III and DSM-III-R”. In: *Archives of General Psychiatry* 46.4 (1989), p. 361.

[76] P. Perry. “Pharmacotherapy for major depression with melancholic features: relative efficacy of tricyclic versus selective serotonin reuptake inhibitor antidepressants”. In: *Journal of Affective Disorders* 39.1 (1996), pp. 1–6.

[77] W. A. Brown. “Treatment response in melancholia”. In: *Acta Psychiatrica Scandinavica* 115.s433 (2007), pp. 125–129.

[78] P. J. McGrath et al. “Response to a Selective Serotonin Reuptake Inhibitor (Citalopram) in Major Depressive Disorder With Melancholic Features”. In: *The Journal of Clinical Psychiatry* 69.12 (2008), pp. 1847–1855.

[79] S. M. Monroe and S. F. Anderson. “Depression: The Shroud of Heterogeneity”. In: *Current Directions in Psychological Science* 24.3 (2015), pp. 227–231.

[80] S. D. Østergaard, S. O. Jensen, and P. Bech. “The heterogeneity of the depressive syndrome: when numbers get serious”. In: *Acta Psychiatrica Scandinavica* 124.6 (2011), pp. 495–496.

[81] G. Parker. “A Case for Reprising and Redefining Melancholia”. In: *The Canadian Journal of Psychiatry* 58.4 (2013), pp. 183–189.

[82] G. Parker et al. “Inching toward Bethlehem: Mapping melancholia”. In: *Journal of Affective Disorders* 123.1-3 (2010), pp. 291–298.

[83] B. Zhang et al. “Altered task-specific deactivation in the default mode network depends on valence in patients with major depressive disorder”. In: *Journal of Affective Disorders* 207 (2017), pp. 377–383.

[84] J. Nelson and C. Mazure. “Ruminative thinking”. In: *Journal of Affective Disorders* 9.1 (1985), pp. 41–46.

[85] B. L. Alderman et al. “Rumination in major depressive disorder is associated with impaired neural activation during conflict monitoring”. In: *Frontiers in Human Neuroscience* 9 (2015).

[86] M. G. Berman et al. “Depression, rumination and the default network”. In: *Social Cognitive and Affective Neuroscience* 6.5 (2010), pp. 548–555.

[87] M. A. Ferdek, C. M. van Rijn, and M. Wyczesany. “Depressive rumination and the emotional control circuit: An EEG localization and effective connectivity study”. In: *Cognitive, Affective, & Behavioral Neuroscience* 16.6 (2016), pp. 1099–1113.

[88] R. M. Hutchison et al. “Dynamic functional connectivity: Promise, issues, and interpretations”. In: *NeuroImage* 80 (2013), pp. 360–378.

[89] C. Savin and G. Tkačik. “Maximum entropy models as a tool for building precise neural controls”. In: *Current Opinion in Neurobiology* 46 (2017), pp. 120–126.

[90] A. Painsky, S. Rosset, and M. Feder. “Memoryless representation of Markov processes”. In: *2013 IEEE International Symposium on Information Theory* (2013).

[91] G. Deco and V. K. Jirsa. “Ongoing Cortical Activity at Rest: Criticality, Multistability, and Ghost Attractors”. In: *Journal of Neuroscience* 32.10 (2012), pp. 3366–3375.

[92] K. Murphy and M. D. Fox. “Towards a consensus regarding global signal regression for resting state functional connectivity MRI”. In: *NeuroImage* 154 (2017), pp. 169–173.

[93] D. Rosenbaum et al. “Amplitude of low frequency fluctuations (ALFF) of spontaneous and induced rumination in major depression: An FNIRS study”. In: *Scientific Reports* 10.1 (2020).

[94] C. Dansereau et al. “Statistical Power and prediction accuracy in multisite resting-state fMRI connectivity”. In: *NeuroImage* 149 (2017), pp. 220–232.

[95] R. G. Miller. *Simultaneous statistical inference*. McGraw-Hill, 1966.

[96] W. Treynor, R. Gonzalez, and S. Nolen-Hoeksema. “Rumination reconsidered: A psychometric analysis”. In: *Cognitive Therapy and Research* 27 (2003), pp. 247–259.

[97] E. I. Fried, F. Coomans, and L. Lorenzo-Luaces. “The 341737 ways of qualifying for the melancholic specifier”. In: *The Lancet Psychiatry* 7.6 (2020), pp. 479–480.

[98] C. V. Day and L. M. Williams. “Finding a biosignature for melancholic depression”. In: *Expert Review of Neurotherapeutics* 12.7 (2012), pp. 835–847.

[99] C. V. Day et al. “Cognitive and emotional biomarkers of melancholic depression: An iSPOT-D report”. In: *Journal of Affective Disorders* 176 (2015), pp. 141–150.

[100] N. Ichikawa et al. “Primary functional brain connections associated with melancholic major depressive disorder and modulation by antidepressants”. In: *Scientific Reports* 10.1 (2020).

[101] X. Cui et al. “Aberrant default mode network homogeneity in patients with first-episode treatment-naive melancholic depression”. In: *International Journal of Psychophysiology* 112 (2017), pp. 46–51.

[102] D. Dai et al. “Ketamine Normalizes the Structural Alterations of Inferior Frontal Gyrus in Depression”. In: *Chronic Stress* 4 (2020), p. 247054702098068.

[103] *Diagnostic and statistical manual of mental disorders: DSM-3*. American Psychiatric Association, 1980.

[104] *Diagnostic and statistical manual of mental disorders: DSM-4*. American Psychiatric Association, 2000.

[105] J. Gerdtz. “Mental illness and the roman physician: The legacy of Soranus of Ephesus”. In: *Psychiatric Services* 45.5 (1994), pp. 485–487.

[106] C. C. Guo et al. “Out-of-sync: disrupted neural activity in emotional circuitry during film viewing in melancholic depression”. In: *Scientific Reports* 5.1 (2015).

[107] S. W. Jackson. *Melancholia and depression: From Hippocratic Times to the present*. Yale University Press, 1986.

[108] N. Kopell et al. “Beyond the Connectome: The Dynome”. In: *Neuron* 83.6 (2014), pp. 1319–1328.

[109] K. Z. LeWinn et al. “An exploratory examination of reappraisal success in depressed adolescents: Preliminary evidence of functional differences in cognitive control brain regions”. In: *Journal of Affective Disorders* 240 (2018), pp. 155–164.

[110] C. S. Lewis. *The problem of pain*. Collins, 1940.

[111] Q. Li et al. “Meta-analysis of cortical thickness abnormalities in medication-free patients with major depressive disorder”. In: *Neuropsychopharmacology* 45.4 (2019), pp. 703–712.

[112] A. B. Nejad, P. Fossati, and C. Lemogne. "Self-Referential Processing, Rumination, and Cortical Midline Structures in Major Depression". In: *Frontiers in Human Neuroscience* 7 (2013).

[113] M. Perrot, D. Rivière, and J.-F. Mangin. "Cortical sulci recognition and spatial normalization". In: *Medical Image Analysis* 15.4 (2011), pp. 529–550.

[114] D. A. Pizzagalli et al. "Reduced Caudate and Nucleus Accumbens Response to Rewards in Unmedicated Individuals With Major Depressive Disorder". In: *American Journal of Psychiatry* 166.6 (2009), pp. 702–710.

[115] P. E. Pormann. *On Melancholy: Rufus of Ephesus*. Mohr Siebeck GmbH and Co. KG, 2008. ISBN: 9783161497605.

[116] D. Rosenbaum et al. "Aberrant functional connectivity in depression as an index of State and trait rumination". In: *Scientific Reports* 7.1 (2017).

[117] R. P. Snaith et al. "A Scale for the Assessment of Hedonic Tone the Snaith–Hamilton Pleasure Scale". In: *British Journal of Psychiatry* 167.1 (1995), pp. 99–103.

[118] T. Takahashi et al. "An MRI study of the superior temporal subregions in patients with current and past major depression". In: *Progress in Neuro-Psychopharmacology and Biological Psychiatry* 34.1 (2010), pp. 98–103.

[119] P. Uhlhaas and W. Singer. "Neuronal Dynamics and Neuropsychiatric Disorders: Toward a Translational Paradigm for Dysfunctional Large-Scale Networks". In: *Neuron* 75.6 (2012), pp. 963–980.

[120] A. Weinberg and S. A. Shankman. "Blunted Reward Processing in Remitted Melancholic Depression". In: *Clinical Psychological Science* 5.1 (2016), pp. 14–25.

[121] C. I. Workman et al. "Subgenual Cingulate–Amygdala Functional Disconnection and Vulnerability to Melancholic Depression". In: *Neuropsychopharmacology* 41.8 (2016), pp. 2082–2090.

[122] M. Yan et al. "Disrupted Regional Homogeneity in Melancholic and Non-melancholic Major Depressive Disorder at Rest". In: *Frontiers in Psychiatry* 12 (2021).

[123] V. E. Zamoscik et al. “Respiration pattern variability and related default mode network connectivity are altered in remitted depression”. In: *Psychological Medicine* 48.14 (2018), pp. 2364–2374.

Publication List

[1] P. R. Regonia et al. "Energy landscape analysis of depressive brain state dynamics". In: *IBRO Reports* 6 (2019).

[2] P. R. Regonia et al. "Modeling heterogeneous brain dynamics of depression and melancholia using energy landscape analysis". In: *Frontiers in Psychiatry* (2021).

Conference List

[1] P. R. Regonia et al. “A neuronal network approach to analyze cooling effect against epileptic discharges”. Presented at the 40th International Conference of the IEEE, Engineering in Medicine and Biology Conference. 2018.

[2] P. R. Regonia et al. “Energy landscape analysis of depressive brain networks using resting state fMRI”. Presented at the 19th Winter Workshop on the Mechanism of Brain and Mind, Hokkaido, Japan. 2019.

[3] P. R. Regonia et al. “Predicting optical band gap of ZnO quantum dots using supervised machine learning”. Presented at the 7th International Symposium on Organic and Inorganic Electronic Materials and Related Nanotechnologies, Nagano, Japan. 2019.

[4] P. R. Regonia et al. “Energy landscape analysis of depressive brain states”. Presented at the 10th IBRO World Congress of Neuroscience, Daegu, Korea. 2019.

[5] P. R. Regonia et al. “Probabilistic machine learning for predicting cytotoxicity of TiO2-(multi)metal (Ag, Pt, Au) nanoparticles”. Presented at the 6th International Conference on Nanoscience and Nanotechnology, Virtual Conference. 2020.

[6] P. R. Regonia et al. “Energy landscape analysis of melancholic depression using pairwise maximum entropy modeling on rs-fMRI data”. Presented at the 44th Annual Meeting of the Japan Neuroscience Society, Kobe, Japan. 2021.